2015

Effects of tissue fixation on Raman spectroscopic characterization of retina

Shaowei Ding
Iowa State University

Effects of tissue fixation on Raman spectroscopic characterization of retina

by

Shaowei Ding

A thesis submitted to the graduate faculty

in partial fulfillment of the requirements for the degree of

MASTER OF SCIENCE

Major: Agricultural and Biosytems Engineering

Program of Study Committee:
Chenxu Yu, Major Professor
Jacek Adam Koziel
Elizabeth Whitley

Iowa State University

Ames, Iowa
2015

TABLE OF CONTENTS

ACKNOWLEDGEMENTS

I would like to thank my committee chair, Dr. Chenxu Yu, and my committee members, Dr. Elizabeth Whitley, and Dr. Jacek Koziel, for their guidance and support throughout the course of this research.

In addition, I would also like to thank my friends, colleagues, the department faculty and staff for making my time at Iowa State University a wonderful experience. I want to also offer my appreciation to my family for their encouragement and to my parents for her hours of patience, respect and love.

ABSTRACT

Raman spectroscopy is a non-invasive and non-destructive tool that has been widely applied in Agricultural and Bio-system Engineering field. It provides a unique "fingerprint" to different chemical, and structural, information at molecular level. Acquisition of Raman spectrum requires a relatively short collecting time and minimum sample preparation, which makes Raman spectroscopy an attractive method for characterizing biological samples.

Since retina is the most exposed part of the central nervous system, irregular protein transformation, or accumulation caused by diseases, can be found at an early time in this area. Because of this reason, Raman spectroscopy is often utilized to analyze samples from specific layers in retina to detect certain diseases, such as glaucoma, Parkinson's disease, and Prion related diseases at early stages.

In order to have a better preservation of tissue architecture and longer storage time, collected retina samples are commonly first fixed by chemical fixative. Typical fixatives include: Modified Davidson's fixative, Bouin's fixative, Ethanol fixative or conventional Formalin fixative. After fixation, samples are then embedded with paraffin to allow for fine sectioning. Every fixating protocol has different ingredients, and there is no universal fixative that is ideal for all the tissue types. Since fixation introduces chemical modification to the tissue samples, it is important to understand what changes it may cause to the Raman spectroscopic characterization of the tissue samples. For best result, four fixation methods are studied and analyzed in this research. The purpose is to identify a mathematical methodology which can be used to remove the background noise produced by each chemical fixative, and to determine how each fixative alters the collected Raman spectra, and in which regions alternation appears. Although this sounds theoretically promising, the actual cellular

structure is more complex. An alternative approach to study the effect caused by fixation is to investigate, with the disease present, if chemical fixation has any impact on the diagnosing result. And if it does, whether this impact can be minimized to improve the accuracy of diagnosis.

CHAPTER I

INTRODUCTION TO RAMAN SPECTROSCOPY

1.1Theory

Theoretically, if electric field is represented by $\overrightarrow{E_0}$ with frequency v_1, the polarization of an illuminated sample with light can be explained by equation 1.1, in which $\overline{\overline{\propto}}$ is the polarizability tensor depending on matter vibrations. $\overline{\overline{\propto}}$ can be expressed as equation 1.2 of normal coordinates. If we combine the two functions, equation 1.3 can be obtained, from which elastic scattering or Raleigh scattering ($v = v_1$) and inelastic scattering, better known as Raman scattering, ($v = v_1 \pm v_{vib}\ with \frac{\partial \propto_{ij}}{\partial Q} \neq 0$) can be predicted based on atomic vibrations.(Amer 2009)

Equation 1.1

$$\vec{P} = \overline{\overline{\propto}} \times \overrightarrow{E_0} \cos(2\pi v_1 t)$$

Equation 1.2

$$\propto_{ij=\propto_{ij}^0} + \left(\frac{\partial \propto_{ij}}{\partial Q}\right)_{Q=Q_0} \times Q\ , Q = Q_0 \cos(2\pi v_{vib} t)\ and\ (i,j) is\ a\ point\ of\ normal\ coordinates$$

Equation 1.3

$$P = \sum_j \propto_{ij} \times E_i = \sum_j \left[\propto_{ij}^0 E_{0_j} \cos(2\pi v_1 t) + \frac{E_{0_j} Q_0}{2} \left(\frac{\partial \propto_{ij}}{\partial Q}\right)_{Q=Q_0} \times [\cos(2\pi(v_1 - v_{vib})t) + \cos(2\pi(v_1 - v_{vib})t)] + \cdots \right]$$

Scattering of light can be categorized into elastic and inelastic. Light that shines on an object is primarily elastically scattered, that is, there is no loss or gain of energy between the incident photon and the scattered photon. When there exists a change of energy, a much rarer

event can occur. The phenomenon is called inelastic scattering, which was discovered by Raman and Krishna. (Raman 1928) This discovery enables fundamental molecular vibrational transitions to be measured at any excitation wavelength, and it can be applied to identify molecular specificity.(Wei-Chuan Shih 2007)

During the coherent one-step process of Raman scattering, one photon is exchanged for another via the interaction with a molecule. Schematically, this process can be viewed as the change to a higher or lower vibrational state through excitation to a virtual state of sample molecules in a vibrational or rotational mode, along with a new photon scattered simultaneously.(Wei-Chuan Shih 2007) In figure 1, two types of scatterings are illustrated. When there is no change of frequency or energy (V0=V0), it is known as Rayleigh scattering. The inelastic Raman scattering can be further categorized into Stokes scattering and Anti-stokes scattering. If the emitted photon is scattered with red shifted frequency, caused by incident photon giving energy to the samples, it is referred to as Stokes shift. Anti-Stokes shift happens when the incident photon receives energy from the already exited molecules, leading to a scattered photon with blue shifted frequency. As shown in equation 1.3, the prerequisite of Raman scattering is to satisfy $\frac{\partial \propto_{ij}}{\partial Q} \neq 0$, This is the selection rule that governs the change of polarizilibility during vibration.

Raman spectrum provides a unique set of fingerprints corresponding to different chemical bonds or molecular structures. When excitation photons interact with molecules in a sample (typically monochromatic light from a laser source), the scattering happens, while the

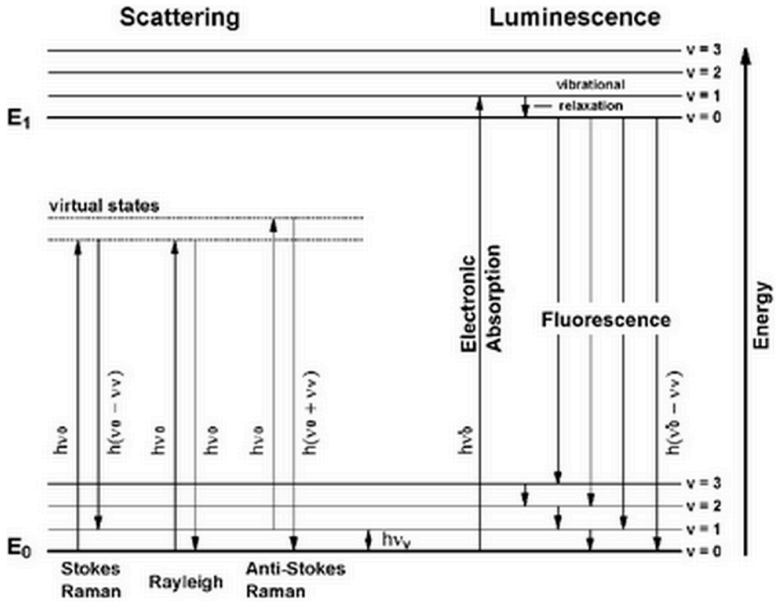

Figure 1 A schematic view of Raman scattering (Collette, 2002) For reproduction of material from NJC: Reproduced from Ref. (Collette, 2002) with permission from the Centre National de la Recherche Scientifique (CNRS) and The Royal Society of Chemistry.

loss or gain of energy is seen as a change in energy of scattered photons. This change, for a particular bond in the molecule, is represented by the appearance of a Raman peak at specific wavenumber, which can be converted to wavelength using wavelength (in μm) = 10000/wavenumber (in cm^{-1}). Its intensity is proportional to the number of scattered photons. A typical mechanism of Raman spectra is shown in figure 1.

1.2 Background on Biological Applications of Raman Spectroscopy

1.2.1 Applications of Raman Spectroscopy

Raman spectroscopy has found applications in many research fields, as it is non-destructive that measurements are derived from ubiquitous chromophores, which gives it an extremely broad range of accessible samples. (Kniggendorf, Gaul et al. 2011) Moreover, this technique is non-invasive and requires minimum sample preparation and small sample volume. Compared to widely-used florescence spectroscopy, Raman spectrum is featured by a wealth of narrow peaks corresponding to specific molecular structures that serve like a set of unique fingerprints and can be related to the tested sample easily. (Richards-Kortum and Sevick-Muraca 1996) These advantages allow the static and dynamic properties of biologically important samples in different environment to be studied and characterized, such as solution, cell cultures, single living cells, cell culture and in tissues including the eye globe. (Richards-Kortum & Sevick-Muraca, 1996)

1.3 Ocular Structure

An eye enables animals to observe their environment and to become aware of changes in their surroundings. Good vision is important for almost every aspect of life, and it enhances the quality of life. The loss of vision causes not only changes in living but also habits that might results in psychological distress and reduction in the living quality.(Abateneh, Tesfaye et al. 2013)

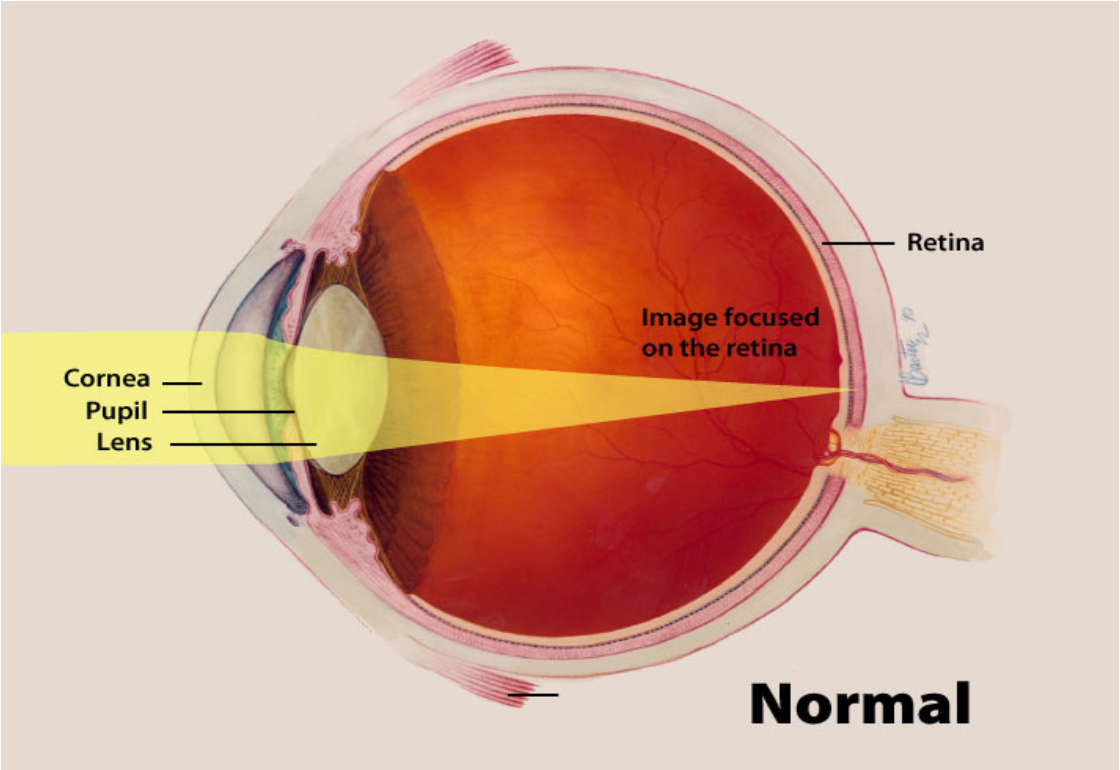

Figure 2. the refraction of incoming light occurs at the cornea with an index of refraction of 1.38, and that number is much bigger than that of the surrounding air. Based on the difference, cornea is shaped as a double convex lens. The ciliary muscle has the ability to alter the shape of the lens or the amount of contraction, which changes the focal length of the cornea length system. Since the object is located at more than 2 focal length from the lens, the image is produced as inverted, reduced in size and real on the retina surface(Henderson 1996). (National eye institute)

The eye receives light from the emission or reflection of objects that passes through its area of photo reception (Figure 2). The eye consists of various tissue components assembled into structures that transmit light signals to photoreceptors, which subsequently send electrical signals to the brain. Photoreceptors are photon-detecting neurons that can convert light energy into an electrical stimulus. Once the light signal is processed in the retina, the electrical signal is then sent back to the visual cortex of the brain. (A.Samuelson 2007)

The eye has three structural layers. The exterior coat, called the fibrous tunic, is divided into two components, the cornea and the sclera. The middle layer is composed of the choroid, ciliary body, and lens. This layer is blood-rich and the intrinsic muscles regulate the shape of the lens and the size of the iris.(Alcamo 2009) The third, interior layer in the global structure is an embryological extension of the brain. Because of this reason, the nervous tunic is morphologically and physiologically intertwined with the brain. (Samuelson, 2007) This includes the retina and the optic nerve. When light penetrates into the eye, rods and cones in the retina receive the photon and transform it into an electrical signal. These two types of photoreceptors are located in the inner layer of the retina, a highly structured cellular network, where bipolar cells, ganglion cells, horizontal cells, Müller's cells and amacrine cells interconnected with each other to deliver impulses to the visual centers of the brain, through the optic nerve, for further vision interpretation.(Alcamo 2009)

1.3.1 Retinal Structure

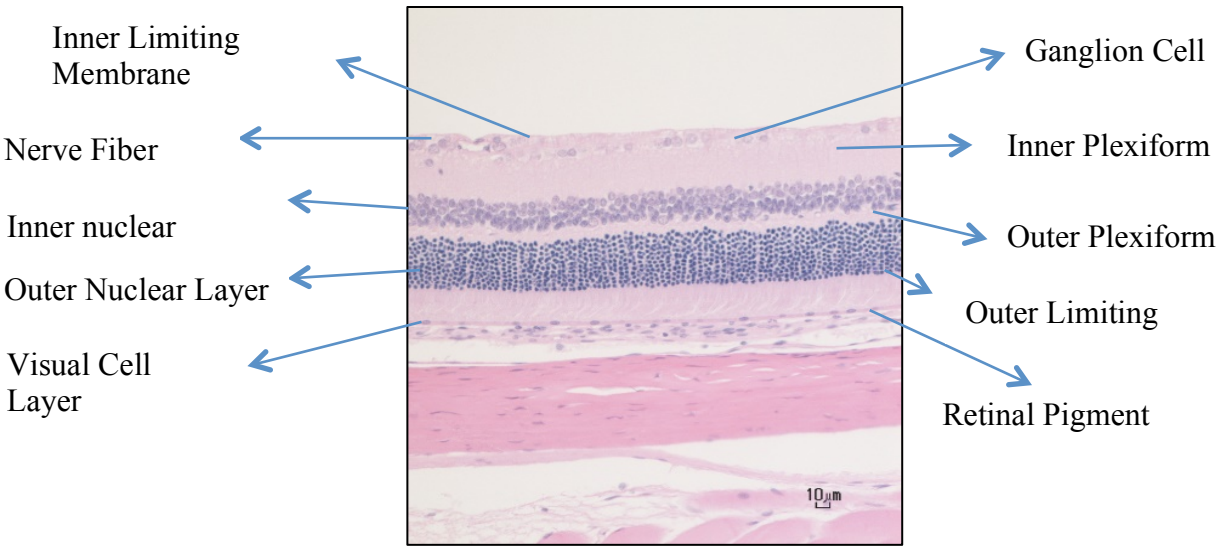

Figure 3. Retinal Anatomy. This image shows the central region of retina from a Fisher 344 rat. Hematoxylin and eosin stain. Image courtesy, Dr. E. Whitley

As a derivative of the forebrain, the retina contains photoreceptors that transmit electric impulses through the optic nerve to the central nervous system for further processing and interpretation. (A.Samuelson 2007) There are ten layers housing three sets of highly ordered neurons from the outside inward (Figure 3). These layers are made up of the retinal pigment epithelium (RPE), neurosensory retina, visual cell layer, outer limiting membrane, outer nuclear layer, outer plexiform layer, inner nuclear layer, inner plexiform layer, ganglion cell layer, nerve fiber layer, and an inner limiting membrane. The optic nerve is directly attached to the brain (Figure 4).(A.Samuelson 2007)

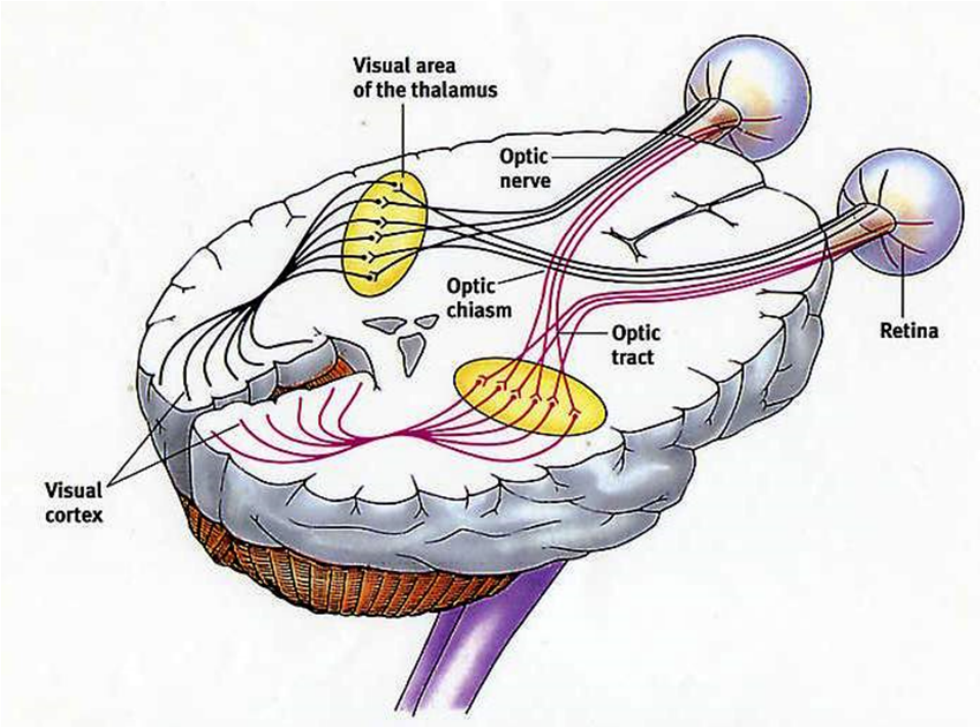

Figure 4. the optic nerve connects to the visual area of the thalamus and the visual cortex in the brain. (Harris)

1.3.2 Retinal Structure-Function Relationships

The retinal pigment epithelium (RPM) is an extension from the out layer of the optic cup, and it is firmly attached to choroid, but loosely adhered to the photoreceptors. The RPE functions are to transport nutrition from the choriocapillaris to the outer layer of retina.

Visual cell layer is home to the rods and cones, which are the outer portion of rod and cone photoreceptor neurons and exist in the visual cell layer where they are packed tightly to receive incoming light signals. Once a photon is absorbed, the signaling within the dendritic process of the photoreceptors is set in motion, where physical energy is transformed into nervous impulses.(Warwick 1976) Two cells function differently because of their shape: In order to detect motion and shapes of objects, rod

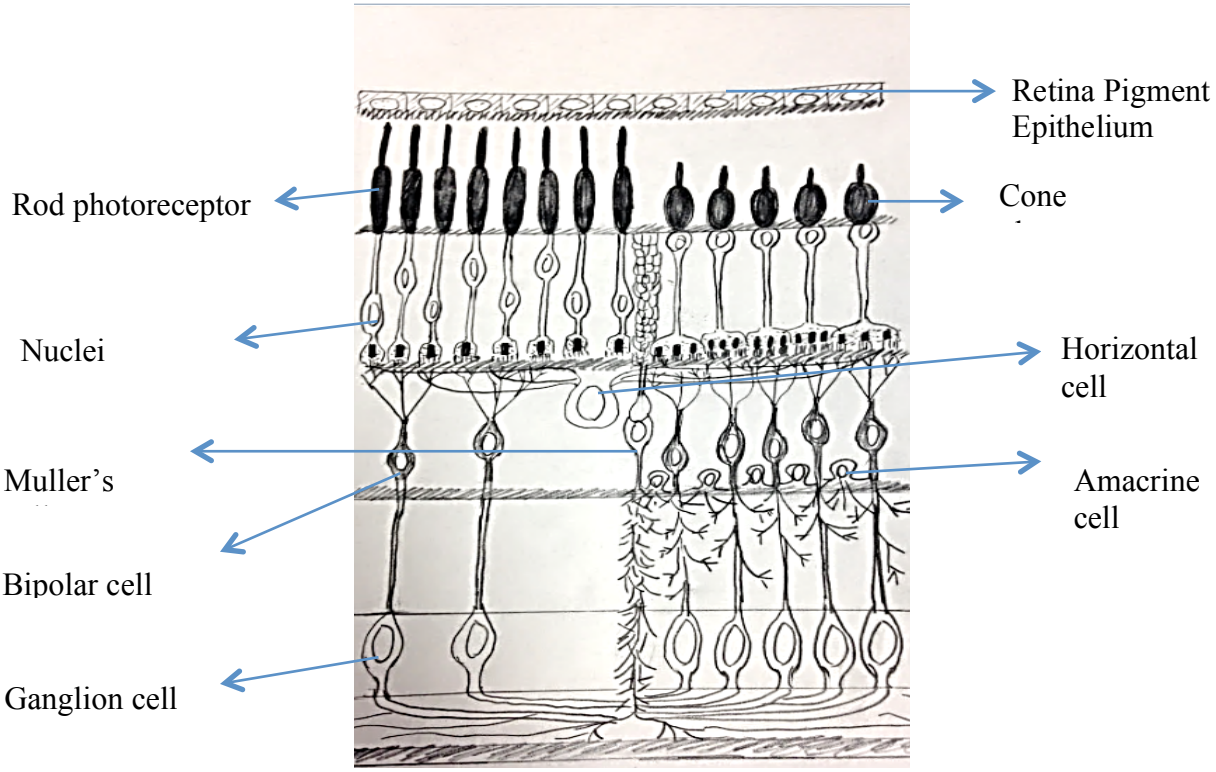

Figure 5. Retinal visual pathway. Rods (left) and cones (cones) are plotted separately for better explanation. The outer segment of a rod cell is longer than the cone's, and rod attaches to its nuclei thought a thin outer fiber. The cone cell connects to the nuclei and then the fiber.

cells are more slender as well as more sensitive to light than the adjacent cone cells. As a result, the rod cells function better in the dark environment. In contrast to rods, cones are useful during daytime or other well-illuminated environments where they can capture reoccurring signals and are sensitive to a specific range of light waves. This feature enables cones the ability to produce color vision with good acuity.(A.Samuelson 2007)

The outer nuclear layer is composed of nuclei of the rods and cones. Rods have round granules that consist of almost nothing but nucleus with little protoplasm around them. Cones, with shorter fiber, have larger and oval shaped granules that connect closely to the outer limiting membrane.(Warwick 1976)

The outer plexiform layer contains the terminal portion of the rods' and cones' axons, they are filled with dendrites of bipolar and horizontal cells (A.Samuelson 2007). Bipolar cells function as a communication channel between the rod and cone cells to the ganglion cells, and horizontal cells display interconnection among photoreceptors. On average, each spherule of rods has connection to four dendrites of horizontal and bipolar cells, while cones' pedicles have about 25 connections to horizontal and bipolar cells. Additionally, bipolar dendrites make simpler contacts on the cell membrane of the pedicles with up to 500 connections. This complex synaptic cross-connection is functionally important, because it is through these pathways that rods and cones are able to excite the visual pathways.(Warwick 1976)

Inner nuclear layer is home to the bipolar neurons, the horizontal neurons, the amacrine neurons, the somata of the cells of Muller and capillaries of the blood vessels.(Warwick 1976) In this layer, bipolar neurons synapse with photoreceptors and receive impulses generated by them. Horizontal neurons regulate the communication between the rods and the cones as well as bipolar cells. Those bipolar cells can synapse with the ganglionic neurons, which contains axons

that extend to form the optic nerve.(Alcamo 2009) Their communication is controlled by Amacrine cells transmitting signals from visual cells to the ganglion cells. Muller's cells serve as supportive cells for the retina and tend to enclose more cytoplasm. Capillaries of this layer serve to provide the retina with a vascular supply, delivering blood to the photoreceptor layer, where it is free of any branches from the central retinal vessels.(Hollyfield 2010) Similar to the outer plexiform layer, complex synapse networks are present in the Inner plexiform layer zone: There is a junction between the first and second order sensory neurons of the visual pathway, as well intricate synapses among bipolar, ganglion and amacrine cells. This cell layer is the second synaptic layer and the final stage for visual processing inside the eye globe. The terminal of bipolar cells' axon collects information from the outer plexiform layer to the neuropil of the inner plexiform layer(Kolb 2007), and amacrine cells alter this signal to ganglion cells. This cellular signal is initially separated into different streams within bipolar cells, where different pathway are formed to convey different information.(Lukasiewicz 2013) Additionally, inner plexiform layer shows a subdivision made by amacrine cells and the dendrites of the stratified ganglion cells.

The ganglion cell layer contains ganglion cells, neuroglial cells and blood vessel. Ganglion cells, with a single dendrite, vary greatly in shape, are multipolar nerve cells. There are three different types ganglion cells primarily based upon the arrangement of dendrites and different cells they synapse.(Warwick 1976)

Nerve fiber layer consists mainly of the axons of the ganglion cells, and fibers usually locate parallel to the surface of the retina. This arrangement is highlighted by special stains, such as Hematoxylin and eosin stain, demonstrating that it is different from the arrangements of the plexiform layers.

Interestingly, some animal species have a special part called the tapetum lucidum, which represents a significant example of adaption of cell and tissue to a dim light environment. It functions to increase the retinal sensitivity and light available in a low illumination environment. When there is high concentration of pigment but devoid of pigment overlying the choroid, which contains the tapetum, allows the RPE to only permit light to hit the tapetum and reflect it back to light signal receptors. (Ollivier 2004)

1.4 Chemical Considerations for Retina Sample Collection

For the applications of imaging technologies in biological, medical and pathological fields, fixation is an important tool and allows extended storage time of biological aggregates such as tissues or bacterial communities, while keeping unaltered properties that are under study. (Kniggendorf, 2011) It mainly has four basic functions: stabilize cellular structure and morphology, disable proteolytic enzymes, strengthen tissues for further processing and protect samples from contamination and decomposition.(Hassel 1974) However, the impact of fixative on samples using common fixation methods has not been given enough consideration, and surprisingly, there are only a small number of published articles that discussed the effects caused by commonly applied fixative protocols in the molecular or cellular scale in details. (Kniggendorf, 2011)

With tissues promptly immersed in the chemical solution, common volume ratio of tissue to fixative is usually 1: 20, but less fixative can be used when a shaking device is applied for fresh tissue, or in other case, the fixative is replaced during the fixing period. (Morawietz, Ruehl-Fehlert et al. 2004) In order to see how significant the effect that chemical fixatives can

cause on the Raman spectroscopic features of the tissue samples, four chemical fixations, including 10% Neutral Buffered Formalin Fixative, Bouin's fixative, modified Davidson's fixative and 70% ethanol fixative in this research are studied, and the control group is frozen fixed sample, which is a kind of physical fixation which does not introduce significant chemical modification to the tissues.

1.4.1 10% Neutral Buffered Formalin Fixation

Change of histopathology can be further evaluated via immunohistochemistry in toxicological studies, which has been conducted on samples mostly fixed by formalin. (McKay, 2009) For most cellular targets, 10% Neutral Buffered Formalin fixation has been widely applied with broad specificity. This is a conventional fixation protocol: Formaldehyde is a water soluble, colorless, toxic, and pungent gas, and the fixation works by it reacting with primary amines on proteins and nucleic acids to form partially-reversible methylene bridges, but it causes artificial cellular shrinkage and lowers the quality of nuclear and cellular resolution of retina.(Hassel 1974)

1.4.2 Bouin's Fluid (BF)

Bouin's fixative is consisted of picric acid, acetic acid and formaldehyde: Picric acid penetrates slowly and forms picrate with basic proteins by precipitating proteins. It is a good preservation tool for glycogen, although may cause tissue shrinkage. (Latendresse, Warbrittion et al. 2002) With rapid penetrating rate, acetic acid coagulates nucleic acids but does not fix proteins, and it is a good method to fix chromosomes. (Latendresse, Warbrittion et al. 2002) Acetic acid produces swelling in tissues, which can be used to reduce the shrinkage produced by picric acid. And Formaldehyde, a non-coagulative fixative, forms cross-linkage in proteins and

has relatively slower penetrating rate. (Latendresse, Warbrittion et al. 2002) It is recommended by most recent revisions of regulatory guidelines for testing effects of chemicals on reproduction, that Bouin's fluid, even causing health and safety hazard and waste problems, is still better than formalin solutions in terms of detailed morphologic preservation. Other disadvantages of BF include labor intensive and multiple rinsing needed for picric acid removal. (McKay, 2009)

1.4.3 Modified Davidson's Fixation (mDF)

Davidson's fixative is considered to be the optimal fixative in terms of preserving eye morphology, since the eye globe has a complex structure, requiring consistent penetrating rate from a single fixative, and needs to be fixed as a whole. (McKay, 2009) Similar to Bouin's fixative except that picric acid is replaced by alcohol, this fixation is made from acetic acid, alcohol and formalin, and it is a rapid penetrating, simple to use without causing safety issues or disposal problems compared to traditional formalin protocol. (Kelder, Inberg et al. 2008) In this method, alcohol can denature proteins by breaking the hydrogen bonds and the tertiary structures. As picric acid is absent, alcohol functions similarly but with a faster penetrating rate, resulting in excessive shrinkage which can be counteracted by acetic acid. The adjustment of DF to mDF is a much lower alcohol and acetic acid concentration and a much higher formalin concentration. (Latendresse, Warbrittion et al. 2002) Both methods have a poor quality of lenticular fixation with inconsistent staining in central layers. Even mDF produces detachment of retina and worse preservation of the sensory endings of photoreceptor cells, the fixed samples still have acceptable fixation for cornea and retina. (McKay, 2009)

1.4.4 95% Ethanol Fixation

Alcohol functions by precipitating large protein molecules and is good for cytological preservation. Ethanol can permeablize cells in the sample but causes serious shrinkage. (Hassel 1974)

1.4.5 Frozen Fixation

There are scenarios when some samples with antigens are too sensitive to chemical fixation or organic solution during deparaffinization. These samples can be embedded in cryoprotective embedding medium like OCT, and then get snap-frozen and immersed into liquid nitrogen for storage.

1.5 Analysis of Raman Spectral Data

The analysis of data based on multivariate statistical analysis has been widely explored for Raman spectral data, and it is proven to be highly effective in distinguish spectral features with high sensitivity and specificity associated with disease diagnosis. (Amer 2009) However, analysis of spectral data can be complicated. Even specimens are prepared well, the device is calibrated carefully and scanning parameters are optimized to reach the best measurement, the recorded spectra still consists of many sub-spectra, including spectra from the sample, the instrument and the disturbance in the environment. The general term, noise, is mainly from the last two resources, and beside this noise, the spectra can also be categorized into real spectra and noise spectra. The noise spectra are collected from impurities or defects in the sample.(Zhang 2012)

In order to obtain the real spectra, analysis of components and their spectral features in the specimen needs to be conducted, and the noise needs to be either eliminated or at least minimized, through data processing methods such as normalization, smoothing, baseline correction, etc. Furthermore, for the comparison of the differences among spectra of different samples, statistical techniques and classification methods can be applied, such as Linear Discriminant Analysis and Least Square Support Vector Machines. Nevertheless, several cross validation methods can be used to mathematically check the classification or comparison accuracy.

1.5.1 Normalization

In order to make a valid biological comparison, the first step for data preprocessing is usually normalization, which adjusts the individual peak intensities to balance every spectrum appropriately. (Quackenbush, 2002) It is preferable to scale the spectrum between 0 and 1, since it provides a better visual comparison and a valid and accurate data classification. Normalized peak areas can ensure correct quantitation, and common methods include Area Normalization, and the Maximum Intensity Normalization.

1.5.1.1 Area Normalization

Area Normalization method scales Raman intensities to area/area ratio in the range of [0, 1], where the denominator is the overall area under the Raman spectrum. This method takes the width of peaks into consideration, and the maximum intensity normalization method only focus on the Intensity.

1.5.1.2 Maximum Intensity Normalization

Intensities are proportional to the concentration of the active species in the sample. In order to take a closer look at the intensity value and compare a large amount of samples, maximum intensity normalization method is applied by dividing intensity by the maximum intensity value, which scales the intensity to a range of 0 to 1. This can be explained by equation 1.4 below.

$$Equation\ 1.4 \qquad \text{Normalized } Y_i = \frac{Y_i}{Y_{max}}$$

1.5.2 Smoothing

Smoothing is a kind of fundamental preprocess for Raman spectral data, which is to "sand away the rough edge" from a dataset. From another point of view, smoothing reduces variances in data that has no assignable cause and to thereby make systematic feature of the data more apparent.(Hart 1997) The most widely used method for smoothing is called moving average or window estimate, as seen in figure 6. Suppose we have a spectrum with intensity Y and wavelet X, and for each X, consider the interval [X-H, X+H], where H is a small positive number. X=Y-H and X=Y+H, forming two lines, create a window and lie within the (X, Y) plane. This window can move anywhere within the wavelength range to compute an estimate, r, at any point. The r value is the average of all the Y values in a window.

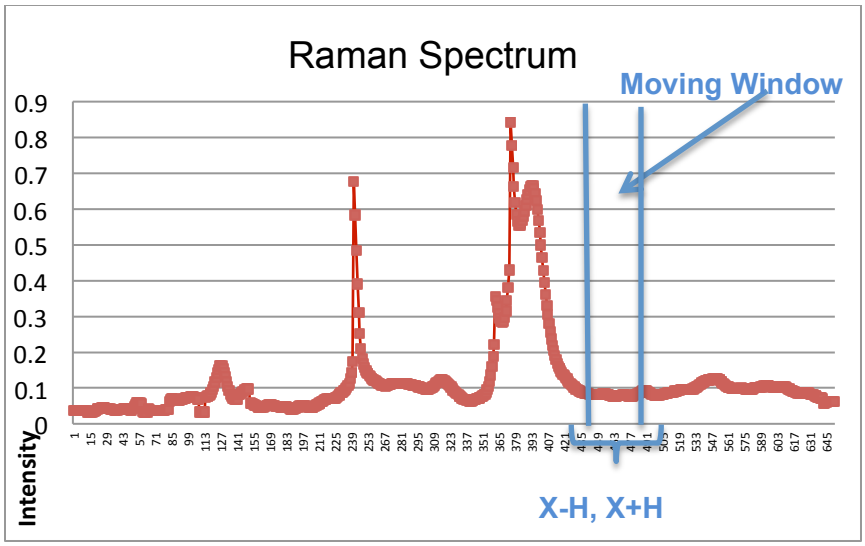

Figure 6. Local Averaging Method

The blue box can be moved anywhere, and the average of all Y values in the window is computed as the smoothed point.

1.5.3 Baseline Correction

Raman spectra collection is seriously affected by the fluorescence background, which should be suppressed to perform further qualitative and quantitative analysis. There are mainly three types of background existing in Raman spectra, consisting of Rayleigh scattering, long Stokes Shift fluorescence, and short Stokes shift fluorescence effects. For a typical Raman Spectra, the fluorescence noise appears as smooth features such as offset, linear baselines, or exponential curves.(Zhang 2009)

Every Raman spectra has x-axis for Wavelength and y-axis for Intensity. In order to better explain this theory, Intensity (Y) can be models as equation 1.6, which is the sum of background b and the real spectrum R, multiplying a blurring function c, with the noise n added to the product.(GEORG SCHULZE 2005) Real spectrum R is the value received after data preprocessing, and it can be written as Equation 1.5.

$$Equation\ 1.5 \qquad Y = (R + B) * C + N$$

$$Equation\ 1.6 \qquad R = \frac{Y - N}{C} - B$$

There are mainly three background correction algorithms in Raman spectral analysis, including polynomial fitting, wavelet transformation, and to calculate the derivative spectra.(Zhang 2009) For these three techniques, polynomial fitting, belonging to signal removal method (SRM), involving the estimation of the background B; Wavelet Transformation requires information of the frequency; and the derivative spectrum doesn't need any explicit knowledge of C, B and N.(GEORG SCHULZE 2005)

1.5.3.1 The Modified Polynomial Fitting

Polynomial curve fitting can keep the contour and intensities of the real Raman spectra. As a result, this feature makes this method fairly good for fluorescence noise correction. What the polynomial fitting does is first to fit a polynomial of order n, and any difference between the raw spectra and the calculated one will be removed. As seen in 1.7, for a function can be separated into a peak Yp(x) and a background Yb(x), the fitted spectrum Y_i is calculated by minimizing $[Y_i - Yp(x_i) - Yb(x_i)]^2$, which is a value consistently underestimated by the fitted curve (Bevington, 1969). Function 1.8 is the general equation for a spectrum. (The spectra is mathematically represented by a Poisson's distribution for a better explanation)

$$Euqation\ 1.7 \qquad \frac{\partial}{\partial aj}\sum\left\{\frac{1}{\sigma i^2}[Yi - Yp(x_i) - Yb(x_i)]^2\right\} = 0$$

$$aj = a, c$$

$$Euqation\ 1.8. Y(x) = ae^{-bx^2} + c$$

This iteration is run by minimizing the least square value until convergence.(Leger 2006) However, this method is not 100% efficient, the subtracted value includes both the background and the Raman peaks, which make the corrected spectra derive many negative values under the zero axis. (Mahadevan-Jansen 2003) The further modified polynomial curve fitting was developed by Lieber and mahadevan-Jansen in 2003, called LMJ method, which assigns raw values to data points with an intensity value larger than the respective pixel value. Thus the background can be eliminated when the there are no more data points bigger than respective smoothed spectrum intensities.(Mahadevan-Jansen 2003)

1.5.3.2 Derivative Spectra

The derivative spectrum is a well-known method for spectral data analysis, and both the first and the second derivative spectra are widely applied for data analysis. This method has the advantage of the application for quantification, as the result is proportional to the sample concentration. Nevertheless, this technique does not require many preprocessing steps, and it enables the detection of peak position and the estimation of peak width.(Zhang 2009) Calculation of the first derivative spectra can efficiently remove steady offsets in the raw data, and it helps to visualize the change of the intensity. Furthermore, this technique discriminates against slowing changing spectra component.(GEORG SCHULZE 2005) Compared to the first derivative, the second derivative calculation leads to the further removal of linear drifts in the raw data set. (Leger 2006)

1.5.4 Classification

After pre-processing, classification is the next step for Raman spectral data analysis in terms of diagnostic applications. Both unsupervised and supervised learning are common methods for classification, and several methods have been developed.(Alexandros Kyriakides1 2010)

1.5.4.1 Principal Component Analysis (PCA)

Principal component analysis is a common multivariable analysis method, and it is designed to explain the total variances in a dataset by taking p variables and the combination of their indices that are uncorrelated in order of their importance.(Manly 1944) P variables are represented by X(1), X(2), X(3)….X(p) and indices are represented by Z1, Z2, Z3....Zp (the principal components, or PCs). The relation of Xs and Zs can be explained by equation 1.9. PCs are orthogonal (i.e., independent) to each other, which means they are measuring different dimension in a data set. Furthermore, most of the variation in a dataset can be adequately represented by a subset of Z values, and the remaining Zs can be considered as negligible. Thus by transforming data into Z PCs, the dimension of a data set can be largely reduced.

$Equation$ 1.9 $$Z_i = a_i(1)X(1) + a_i(2)X(2) + \cdots + a_i(p)X(p)$$

$$a_i(1)^2 + a_i(2)^2 + a_i(3)^2 + \cdots + a_i(p)^2 = 1$$

$$i = 1, 2, 3 \ldots n$$

1.5.4.2 Least Square Support Vector Machine (LS-SVM)

Least Square Support Vector Machine (LS-SVM), proposed by Suykens and Vandewalle, is a classification method and modification based on the standard of SVM. SVM can find the maximal margin hyper plane between different classes. When data are not linearly separable, SVM can plot the data in a higher dimensional space and then map the hyper plane within the maximal margin space. (Fan and Liu 2013) Compared to SVM, LS-SVM method possesses significant advantages, as it adopts the structural risk minimization theory, causing the global optimal solution uniquely obtained by solving a set of linear equations, and over-fitting is less likely to happen. (Huo, Zhu et al. 2006) LS-SVM can be adopted in both linear and nonlinear regression as well as multivariate function estimation,(Suykens 2002) and it applies a linear set of functions instead of a quadratic programming to obtain the support vectors. Assume a training data set has binary classification, with selective sig2(σ2) and gam(γ) tuning parameters, the algorithm can be explained as function 1.10 .(Shao, Cen et al. 2011) In this equation, b is the bias factor, K()is the kernel function,α is a LaGrange multiplier (the support vector).

$$Equation\ 1.10 \qquad y(x) = \sum_{i=1}^{N} \alpha_i * K(x, x_i) + b$$

1.5.4.3 Linear Discriminant Analysis

Linear discriminant analysis mathematically assigns a weight for each discriminant variable, and the score can reflect the degree to which weight on that variable differs between groups being discriminant. Consequently, the discriminant scores, also known as discriminant coefficients, evaluate on which variable(s) more groups differ, and the score on which the groups differ the most receives the most weight.(Tinsley 2000)

Functions with weighted linear combinations of discriminant variables can be formed by linear discriminant analysis as shown in equation 1.11 D is the discriminant score, a is the Y value of the interception of the regression line and Y-coordinate, and bi is the assigned weight on each variable or the discriminant coefficient. Since coefficients are derived mathematically to maximize the difference between two groups, the cross validation is a critical step to check the uncertainty within this classification. (2000)This step is significant for the prediction needed for biological diagnosis.

$$Equation\ 1.11 \qquad D = a + b_i X_i$$

i=1, 2, 3… N

1.5.5 Cross Validation

Cross Validation is a statistical method of evaluating and comparing classification results. When running a classification, researchers are intended to maximize the difference between two groups of data, and idiosyncratic features have variations within a group of samples, thus the generalization of the classification has much uncertainty. (Tinsley 2000) Consequently, the utilization of cross validations ensures good classification accuracy while maintaining a optimized separation between target and control groups. Commonly applied cross-validation methods, such as Leave-one-out method and the hold-out method, will be discussed below.

1.5.5.1 Leave-One-Out Method

Leave-one-out method, also known as the jackknife method or K-Fold cross-validation (the special case of leave-one out method), is one of the most widely used cross validation

methods. The theory of it is to remove one sample or one fold out of K folds, and then the rest of samples are used to perform a new classification. With the discriminant function obtained, the taken out sample(s) is (are) then used to run the prediction. This loop is repeated and every sample is randomly selected until each sample (every fold) in the group has been held out for the classification. By performing the leave-out-test, researchers are able to evaluate the stability of various statistics produced by the classification.(Tinsley 2000)

1.5.5.2 The Hold-Out Method

The hold-out method is another cross validation method, which involves splitting the sample into two groups as training and testing sets. Data separation is randomly processed, typically with two thirds of the samples marked as training set and one third of the data marked as testing set. The supervised classification is first run using the training group, from which a discriminant equation can be derived, and the accuracy of the hit rate within the testing group represents the prediction accuracy for newer samples.(Tinsley 2000) This method features the independent training and testing data, thus it avoids over-fitting or overlapping between two data sets, providing a more accurate estimate for the generalization of the algorithm. However, the result might be affected by the choice for the data separation, which may lead to skewed results.(PAYAM REFAEILZADEH 2008)

1.6 Research Objectives

The effects caused by chemical fixatives in Raman spectroscopy of mice retina are evaluated and discussed in this research, and there are two main objectives:

1) To investigate the feasibility of a mathematical methodology being developed to remove the background noise produced by each chemical fixative, and to determine how each fixative alters the collected Raman spectra, and in which regions alternation appears.
2) To investigate, with the disease present, if effects of chemical fixation can be minimized to not influence the diagnosis results.

1.7 Dissertation Overview

This dissertation is composed of two major parts based on two objectives: in part one, (chapter 2) The alteration to Raman spectroscopic signatures of retinal tissue samples by chemical fixatives, including ethanol, formalin and modified Davidson's fixatives, is investigated, and the feasibility of removing these effects is studied. In part two, (chapter 3), with the application of Bouin's fixative, it is investigated if samples with Parkinson's disease can be distinguished from normal controls.

In chapter 4, summary and conclusion are presented for the entire research work, and future perspective is offered.

CHAPTER 2

CHARACTERIZE EFFECTS OF TISSUE FIXATION ON RAMAN SPECTROSCOPIC SIGNAURES OF RETINA TISSUES

2.1 Introduction

Chemical fixation is important to preserve tissue morphology, which is routinely adopted when there is a need to store biological specimens for a longer time. In this study, three common fixation methods using modified Davidson's fixative, ethanol fixative and conventional formalin fixative are investigated in comparison with frozen fixed tissues as controls (i.e., no chemical modification to the tissue samples). The goal of chapter 2 is to characterize effects of tissue fixation on Raman spectroscopic signatures of retinal tissues.

2.2 Materials and Methods

Four frozen fixed retina samples, with two section cuts on each gold slide, were used as controls. The controls were frozen fixed subjected to no chemical treatment other than being immersed into 10% phosphate buffered saline (PBS). Three kinds of chemical fixatives, including modified Davidson's fixative (mDF), 95% ethanol (Etoh) and 10% neural buffered formalin, were investigated. Sample were mounted on gold coated slides and immersed into different fixative in a petri dish. Then they were air dried and measured after 4 hours. All samples in this research were randomly selected and provided by Dr. Elizabeth Whitley from the veterinary medicine school at Iowa State University in Ames. The effects on the Raman spectroscopic characteristics of the retina tissues caused by different chemical fixation were analyzed using a dispersive Raman spectrometer (XTR Raman microscope, Thermo Scientific,

Madison, WI) using a 780 nm excitation laser, with a spectral range of 506-3209 cm^{-1}. 20 replications on each sample were measured.

In typical fixation procedure, after treated with chemical fixatives, tissue samples are often embedded in paraffin to allow longer sample storage time and fine section cut (Matsuda, Fujii et al. 2011). To further evaluate the effect of the paraffin on Raman spectral signatures of the fixed retinal tissue samples, three groups were investigated in a comparative study.
In group 1, chemically fixed tissues were paraffin-embedded, 4 mice with 8 eye globes were studied, whose left and right eye globes were fixed as seen in table 1; In group 2, samples from group 1 were washed using the general paraffin washing protocol to remove the paraffin layer, and were subsequently subjected to spectroscopic measurements. In group 3, no paraffin was used after chemical fixation, to completely remove impact of paraffin.

Spectra were preprocessed with smoothing, modified polynomial baseline correction, and peak normalization. Subsequently different groups were classified using support vector machine algorithm. All data were randomly assigned into training and testing groups and cross-validated, to evaluate the classification accuracy.

Table 1.Paraffin embedded samples with different fixatives applied

Mouse	**Location of eye globe**	**Fixative**
A	Left	Formalin
B	Left	Formalin
C	Left	Formalin
D	Left	Formalin
A	Right	Modified Davidson's
B	Right	Modified Davidson's
C	Right	Ethanol
D	Right	Ethanol

2.3 Results and Discussion

2.3.1 Comparison of Paraffin Embedded Samples

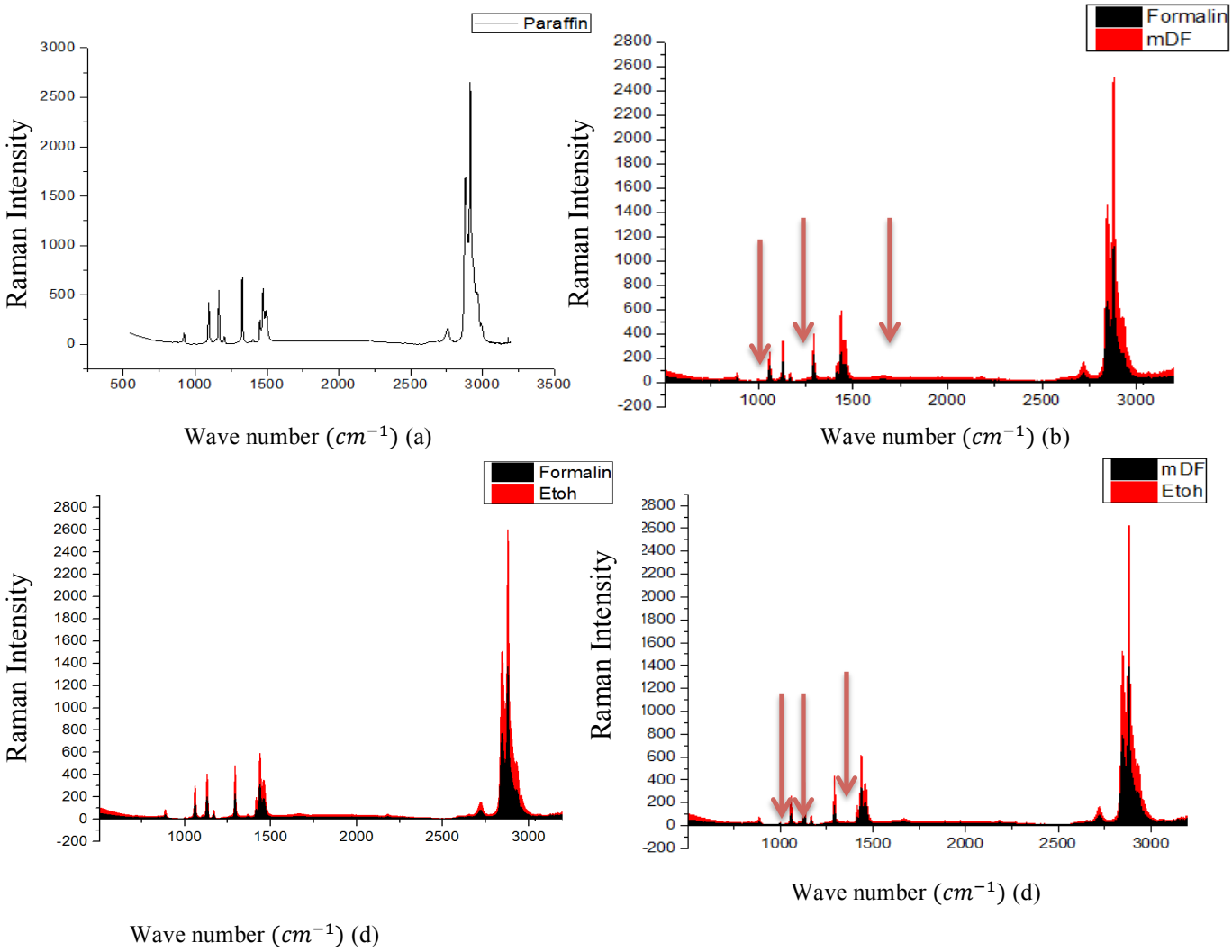

Figure 7. The spectrum of pure paraffin (a) and the mean spectra of chemical fixed samples with paraffin embedded (b) Formalin vs. modified Davidson's Fixative (mDF) (c) Formalin vs. ethanol fixative (Etoh) (d) modified Davidson's fixative (mDF) vs ethanol fixative.(Etoh)

In figure 7(a), the pure paraffin spectrum exhibits signature peaks at 888 cm^{-1},1061 cm^{-1}, 1131 cm^{-1}, 1171 cm^{-1}, 1294 cm^{-1}, 1417 cm^{-1}, 1440 cm^{-1} and 1462 cm^{-1}, due to C-C streching and deformations from CH_2 and CH_3 within paraffin. (Fullwood, Griffiths et al. 2014) Compared to the spectrum of paraffin (7a), chemical fixed samples (b, c ,d) all show signature peaks of paraffin, as the signal of background paraffin is very strong. Even though visual inspection does

not reveal significant differences among the spectra of background paraffin and the chemically fixed samples, some distinguishable features can still be seen in the spectra of chemically fixed samples, such as changes of peak intensity, and the appearance of small new peaks at 1003 cm^{-1}(the C-C symmetric breathing of the aromatic ring in phenylalanine) and 1680 cm^{-1}(Amide I in protein), which are weak but characteristic signals from the retina tissues.

In order to highlight major differences among the three fixation groups, a two-tailed student t –test using P value < 0.05 is utilized to identify peaks with significant differences, and the results are shown in figure 8. Raman spectra of tissues are consisted of bands from different components, i.e., proteins, lipids and carbohydrates, and major peak assignments are listed in table 2.

The major differences from figure 8 can be explained by C-C-N symetric streching from lipids or vibrations of C-O-C rings from carbohydrates at 877cm^{-1}, C-H vibration (1033 cm^{-1}), C-N streching (1128 cm^{-1}), changes of Amide III peak at 1220-1284 cm^{-1} are casued by subtle changes in the secondary structure of protein, and C-H vibration from 1420-1480 cm^{-1}, as well at 2850 cm^{-1}, where change of the CH_2 bond affected Raman spectral intensity.

Existing literatures about the effect of formaldehyde on biological samples suggest that formaldehyde does not change protein content, (Bot. A.C.C. 1989) but it creates a decrease in the SH-stretch Raman signal (2580-2735 cm^{-1}), which is caused by the formation of semithioacetal groups and methylene bridges of SH and paraformaldehyde. (Pearse 1968) Even though formalin is not the most ideal fixation method, as it causes cellular shrinkage and lowers the quality of nuclear and cellular resolution of retina, it is good to serve as a reference to reveal the changes in Raman spectra, due to its simplicity.

Davidson's fixative is considered to be the optimal fixative in terms of preserving eye morphology, since the eye globe has a complex structure, requiring consistent penetrating rate from a single fixative, and needs to be fixed as a whole. (McKay, 2009) Modified Davidson's fixative (mDF) is made from acetic acid, alcohol and formalin (Kelder, Inberg et al. 2008). One would expect that mDF may cause some similar changes in Raman characteristics of the tissues as formalin does, due to the fact that formalin is part of the mDF fixative. This assumption is confirmed by fig.9a, as it suggests that no statistically significant differences can be observed between formalin-treated and mDF-treated samples at ~ 2731 cm^{-1}, which is the signature peak of formalin treatment. Nonetheless, comparison between Raman spectra of mDF treated and formalin treated samples does indicate significant differences caused by acid and alcohol, corresponding to peaks at 877 cm^{-1}, 1003 cm^{-1},1128 cm^{-1},1220 cm^{-1},1420 cm^{-1} and 2850 cm^{-1}, as seen in figure 8a.

Table 2. Peak assignments for Raman spectra (Notingher 2006)

Peak (cm^{-1})	**Assignment**			
	Nucleic Acids	Proteins	Lipids	Carbohydrates
1736			C=O ester	
1680-1655		Amide I	C=C str.	
1617		C=C Tyr, Trp		
1607		C=C Phe, Tyr		
1578	G, A			
1480-1420	G, A, CH def	C-H	CH def	CH def
1342	A, G	C-H		CH def
1320	G	C-H		
1301			CH_2 twist	
1284-1220	T, A	Amide III	=CH bend	
1209		$C\text{-}C_6H_5$. Phe, Trp		
1176		C-H bend Tyr		
1158		C-C/C-N str.		
1128		C-N str.		C-O str
1095-1060	PO_2^- str.		Chain C-C str.	C-O, C-C str
1033		C-H in-plane Phe		
1005		Sym. Ring br Phe		
980		C-C BK str. β-sheet	=CH bend	
937		C-C BK str. α-helix		C-O-C glycos.
877			$C\text{-}C\text{-}N^+$ sym str	C-O-C ring
854		Ring br Tyr		
828	O-P-O asym.str.	Ring br. Tyr		
811	O-P-O str. RNA			
788	O-P-O str. DNA			
782	U,C,T ring br			
760		Ring breath Trp		
729	A			
717			$CN^+(CH_3)_3$ str	
667	T, G			
645		C-C twist Tyr		
621		C-C twist Phe		

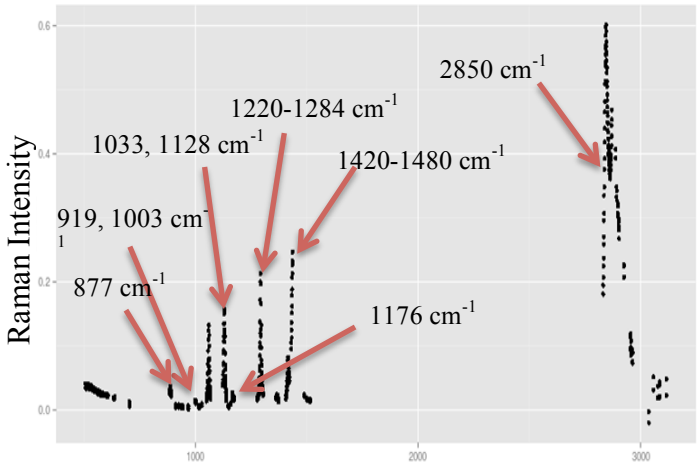

Wave number (cm^{-1})
(a, formalin vs. mDF) Changes due to acid and alcohol

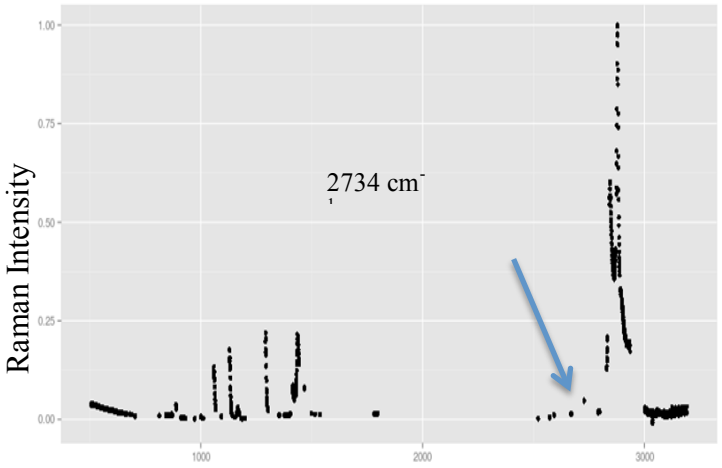

Wave number (cm^{-1})
(b, formalin vs. Etoh) Difference due to alcohol and formalin

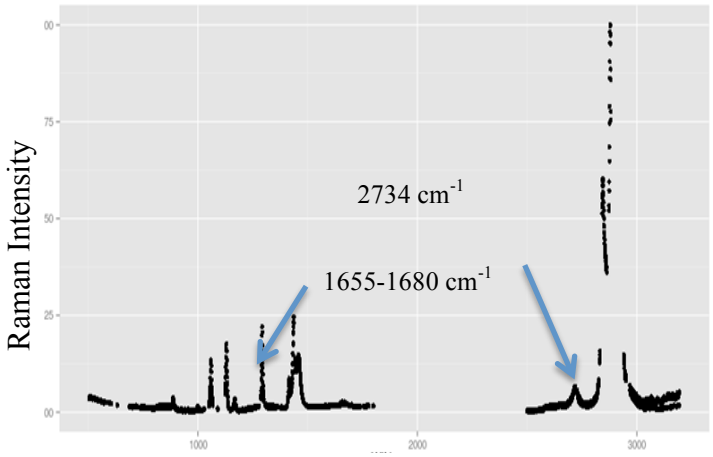

Wave number (cm^{-1})
(C, Etoh vs. mDF) Changes due to acid and

Figure 8. Wavenumbers at which p-value <0.05 (paraffin embedded samples) (a) Formalin vs. mDF (b) Formalin vs. Etoh (c) mDF vs. Etoh

Principal component analysis (PCA) is used for dimensional reduction to facilitate a general classification of targeting groups on a 2D plane. The PC scores are then used for classification at higher dimension. As seen in figure 9, 3 plots from the two PC scores are utilized to display the clustering of spectral data, each data point represents one spectrum measured. As plotted, different fixation methods (i.e., groups) are marked by different color. With SVM, Etoh treated samples and mDF-treated samples are classified into distinguishable classes with highest accuracy (85%); while the classification between formalin/mDF, and Etoh/formalin is less accurate (75% and 80%), but still a high percentage, as shown in table 3. It should be noticed that the formalin/mDF treatments yield the lowest classification accuracy. Given the similarity between these two treatments, this result is as expected. These observations confirm that different fixation methods have large and different impacts on the Raman characteristics of the fixed tissue samples.

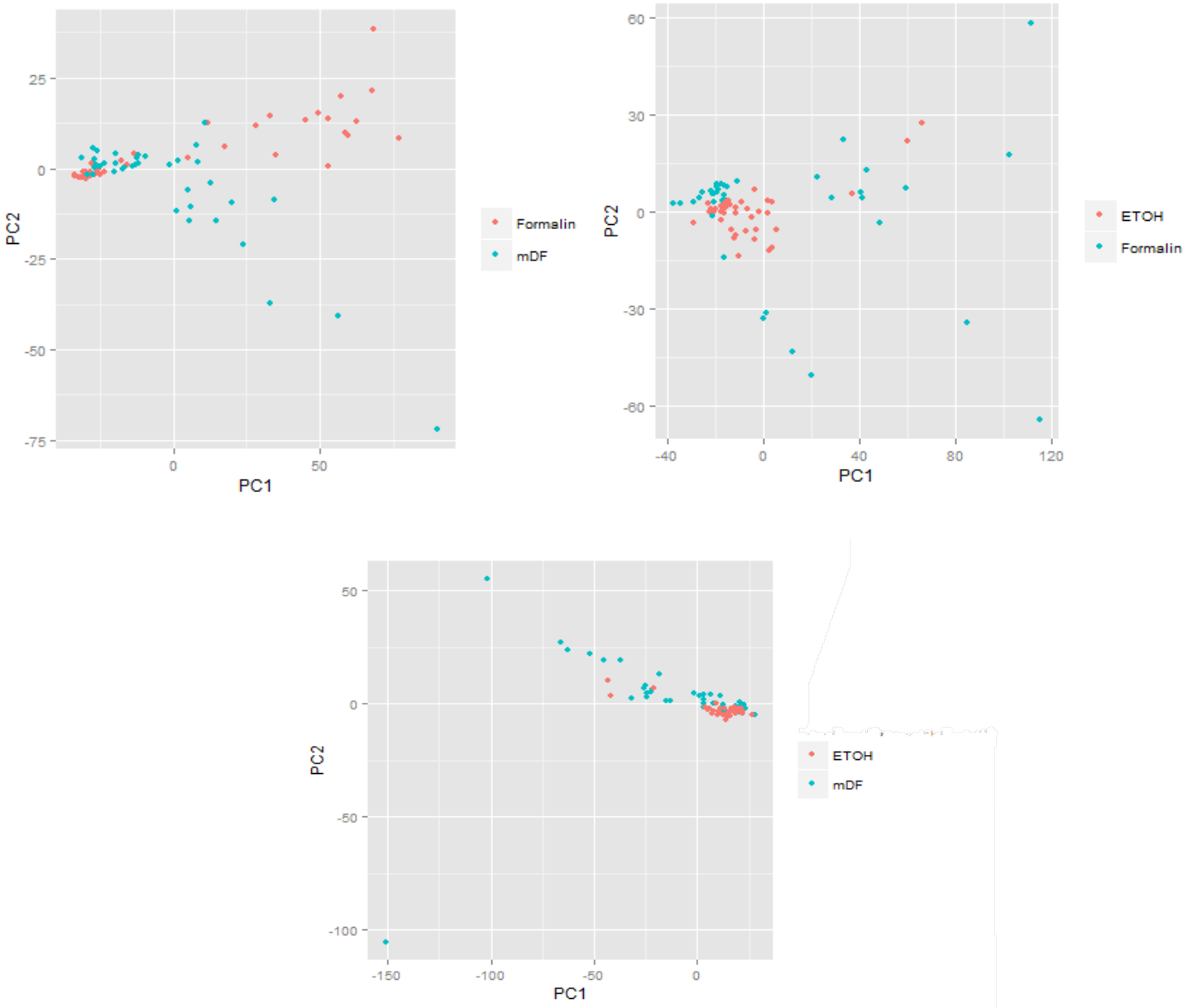

Figure 9. Principal component analyses: a rough classification of samples fixed by different fixation is plotted, as the real distribution is multi-dimensional instead of 2-D. Different fixation is marked in different color, from which formalin and mDF group present clear clustering

Table 3 Classification of paraffin embedded samples

Groups	***Accuracy***
Formalin vs. Etoh	80%
Formalin vs. mDF	75%
Etoh vs. mDF	85%

2.3.2 Comparison of Samples with Paraffin Washed-off

Embedding in paraffin allows fine sectioning for specimen, during the fixating process, paraffin can anchor biological segments and preserve morphological structure better. However, in order to study chemical fixations with less background noise, the impact caused by paraffin in Raman spectra should be studied and minimized as much as possible. Therefore, after spectral measurements were conducted on the paraffin-embedded samples, paraffin was washed off completely using the general paraffin removal protocol as described below.

Step 1: 100% xylene at 60 C for 5 minutes

Step 2: 50% xylene 50% ethanol mixture at 60 C for 5 minutes

Step 3: 100% ethanol at 60 C for 5 minutes

Step 4: 75% ethanol at RT for 5 minutes

Step 5: 50% ethanol at RT for 5 minutes

Step 6: 25% ethanol at RT for 5 minutes

Step 7: Flush under water for 3 times

Step 8: Rinse in PBS for 2 times

Slides are then air-dried for measurements. Figure 7a is the Raman spectrum taken from pure paraffin, and the spectrum has all featured peaks of retinal samples as seen in figure 10 (dewaxed samples), indicating paraffin itself has strong signals. For the sake of this reason, it is important to look at the "raw" signal that is only from biological sample.

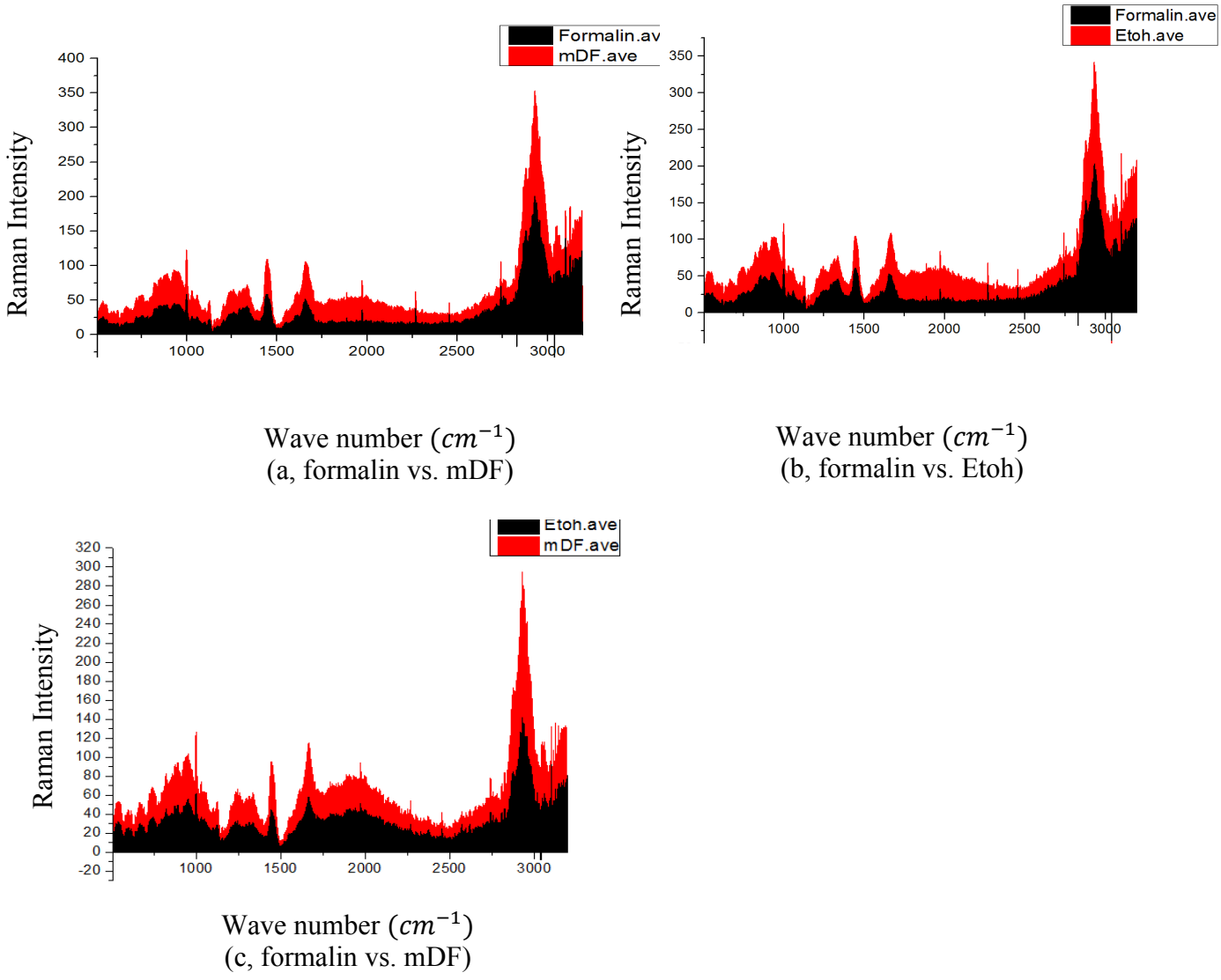

Figure 10. the mean spectra of chemically fixed samples with paraffin removed (a) Formalin vs. mDF (b) Formalin vs.Etoh (c) mDF vs. Etoh

Figure 11 shows peaks (i.e., wavenemubers) with p-values smaller than 0.05 in paired t-tests between data set from different fixation treatments. All peaks, that show significant difference in paraffin embedded samples, are presented here as well. In addition to previously observed signature peaks, a new peak at 1680-1655 cm^{-1} from amide I of proteins can also be identified. Even though the intensity of Raman peaks becomes weaker after the removal of paraffin, two groups of data show more distinguishable features, suggesting that they can be classified with higher accuracy. As shown in figure 11a-c (using t-test). Compared to the formalin set, both Etoh and mDF sets show a wide peak around 1900 cm^{-1}, possibly caused by vibration of C=C bond.

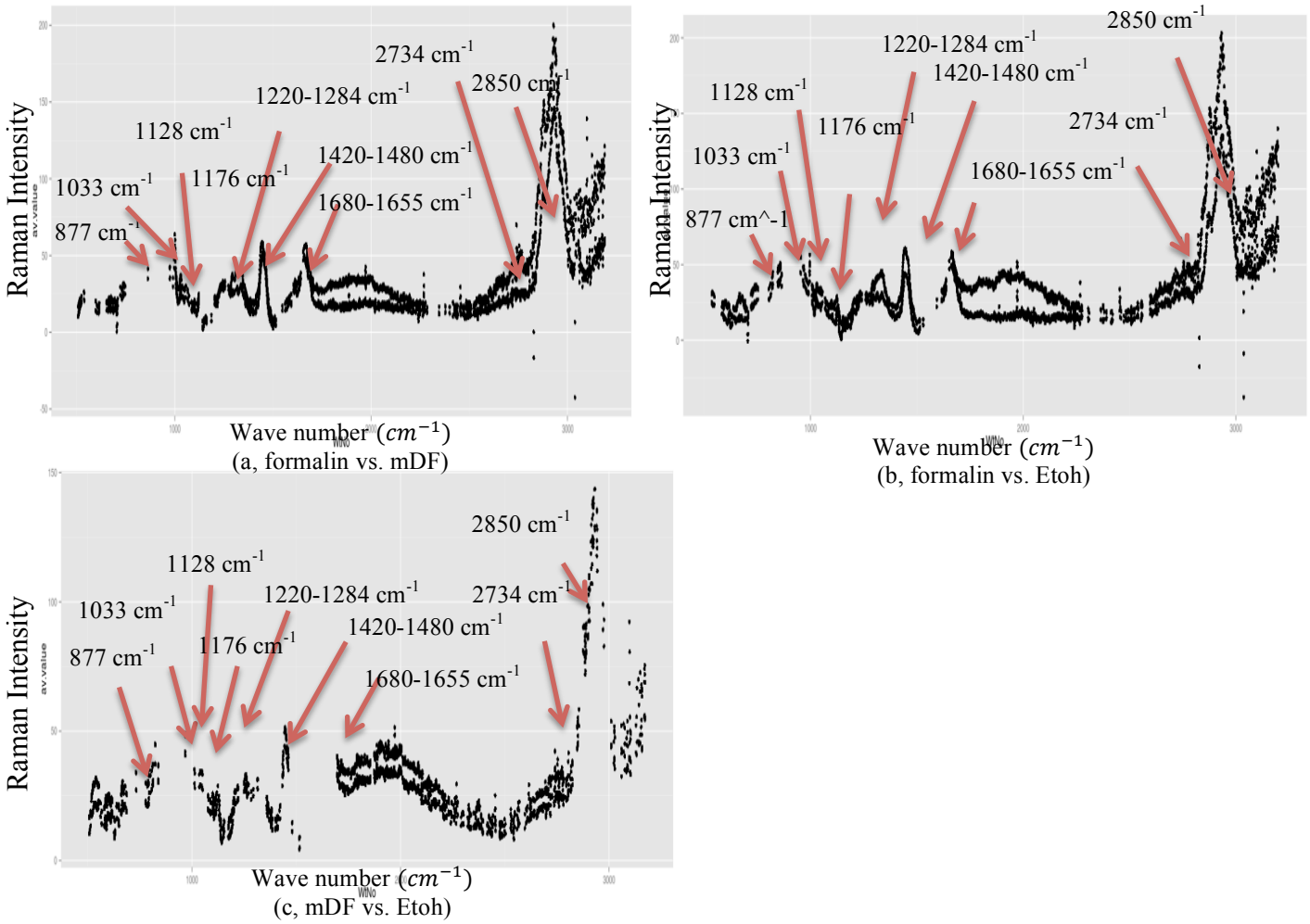

Figure 11 Wavenumbers at which p-value <0.05 (w/ paraffin dewaxed) (a) Formalin vs. mDF (b) Formalin vs.Etoh (c) mDF vs. Etoh

Principal component scores are good indicators of 2-D projection. In figure 12, PC1 and PC2 are plotted to compare the projection of samples fixed by formalin, modified Davidson's and ethanol fixatives, and they are representing a multi-dimensional structure.

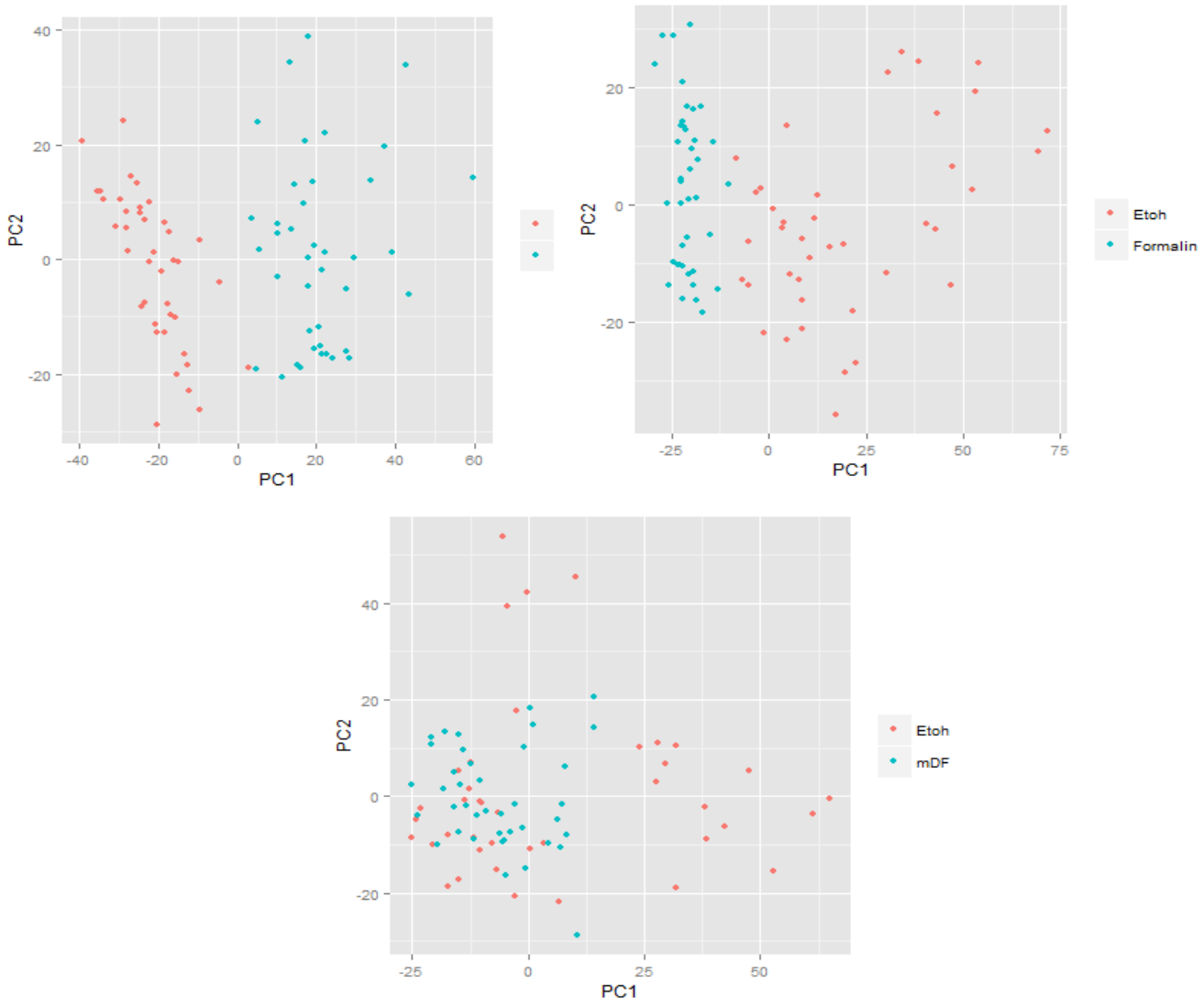

Figure 12 Principal component analyses of samples with paraffin washed off: a 2-D projection of samples fixed by different fixation is plotted, as the real distribution is multi-dimensional. Different fixation is marked in different color, from which formalin groups can be most easily differentiated compared to the other two groups.

Using support vector machines, three sets of data are classified with accuracies listed in table 4. Consistent with the results obtained for paraffin-embedded samples, highest classification accuracy is observed for Etoh/mDF, and lowest for formalin/mDF, due to their chemical similarities. The classification accuracy is improved significantly when paraffin is washed-off, suggesting that the presence of paraffin does significantly affect the characteristics of the retinal tissues, and it should be removed before conducting spectral measurements.

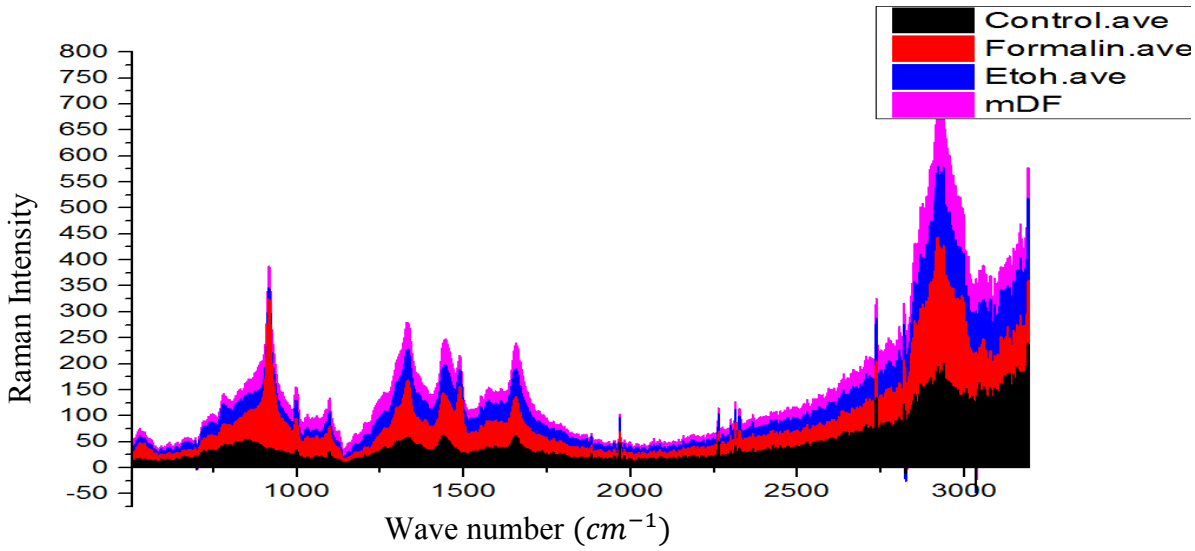

Figure 13 Mean spectra by stacked area of frozen fixed samples with different fixative added (control means frozen samples without fixation, formalin means formalin fixed samples, Etoh means ethanol fixed samples, and mDF means modified Davidson's fixative fixed samples).

2.3.3 Comparison with Frozen Fixed Samples

Using the same pre-processing techniques, the average spectra of frozen fixed samples are plotted in figure 13. Visual inspection shows the absence of peaks at 1480 cm^{-1} and 900 cm^{-1} in the control group, as all other three groups have signals caused by vibrations of C-H bond (1480 cm^{-1}) and the change of α-helix structure (900 cm^{-1}). The peak at 1480 cm^{-1} might be correlated to the presence of secondary structure elements and assigned to the amide II band (ROESSL 2014). The absence of these two peaks in frozen control samples suggests these two peaks observed in the chemically-fixed samples could be related to the crosslinking and denaturation of proteins. While the peak at 215 cm^{-1} can be correlated to the presence of minor ice crystals, with the absence of this peak and a long processing time for fixation, these four samples were confirmed to be completely thawed. (ROESSL 2014)

The PCA graph shown in figure 14 indicates an obvious clustering of control group and ethanol group, while mDF and formalin groups are slightly mixed together. The mixed clusters of mDF and formalin are caused by sharing one common chemical ingredient, formalin, and their minor difference is from acetic acid and ethanol in mDF, which can disrupt cytoskeleton proteins during fixation and compromise variation in Raman spectra.(Howroyd, Hoyle-Thacker et al. 2005) Formalin has been known causing condensation of cellular cytoplasm due to its hyperosmocity, and the resulting alternation is proportional to its concentration. Thus 10% NBF has more condensation of cellular cytoplasm than that of mDF.(Howroyd, Hoyle-Thacker et al. 2005)

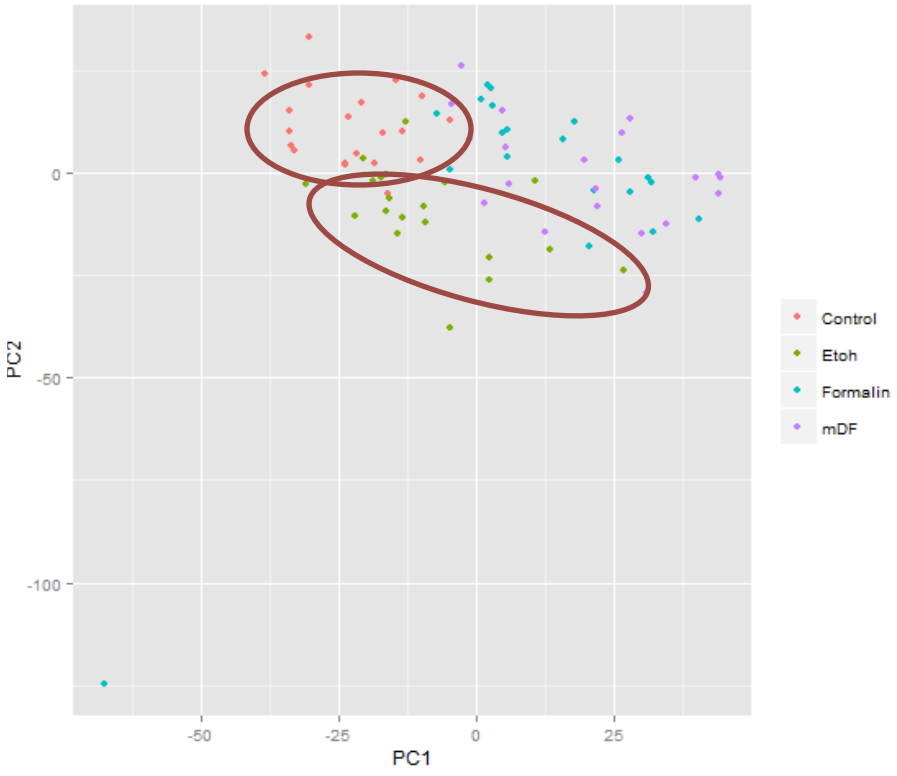

Figure 14 Principal component analyses of frozen fixed samples

2.3.4 Mathematical Correction

Davidson's fixative is considered to be the optimal fixative in terms of preserving eye morphology, since the eye globe has a complex structure, requiring consistent penetrating rate from a single fixative, and needs to be fixed as a whole. (McKay, 2009) Modified Davison's fixative is frequently applied to retinal samples, and here in this section, Raman spectra of mDF fixed samples are compared to that of frozen fixed control samples, with the goal to determine if the background noises caused by chemical fixatives can be mathematically corrected. The general approach is as follows:

Step1: The average spectrum of mDF (mDF.ave) is subtracted by the average spectrum of the control group (frozen fixed);

Step2: The result from step 1 is then divided by "mDF.ave" to calculate the percentage of change at each wavenumber, which indicates in theory what percentage of the original spectra is considered as to be modified by the fixative;

Step3: Using the "percentage of change" that is derived from step 2, to adjust the original spectral data.

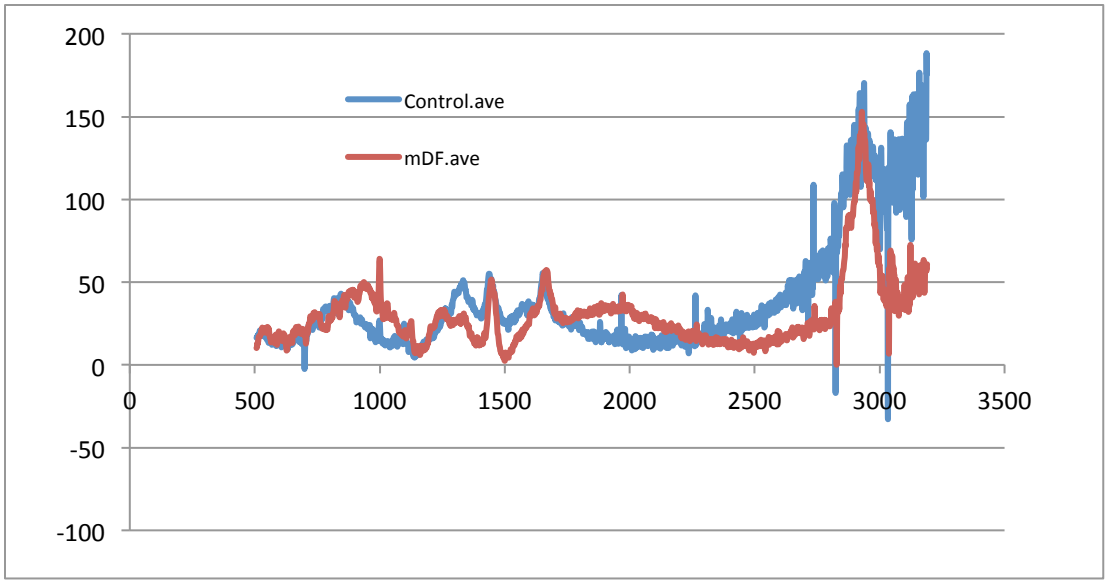

Figure 15 the mean spectra of frozen fixed and mDF samples

The percentage of change with respect to the mean mDF spectrum is shown in figure 16, which clearly shows the actual variation has many extreme values around 2900 cm^{-1}. Using the calculated percentage of difference, a predicted set of mDF spectra can be calculated in figure17. Since the standard deviations among samples are large, consequently the calculated percentage of difference cannot yield an accurate prediction. Moreover, the change of measurement location

within retina also contributes to the inaccuracy in this prediction. Thus the mathematical adjustment is not viable for future prediction of chemical alteration in Raman spectra. However, it still shows a clear peak at 1490cm^{-1} that can be ascribed to the change of protein structure, DNA/RNA or lipid. (Beattie, Finnegan et al. 2012)

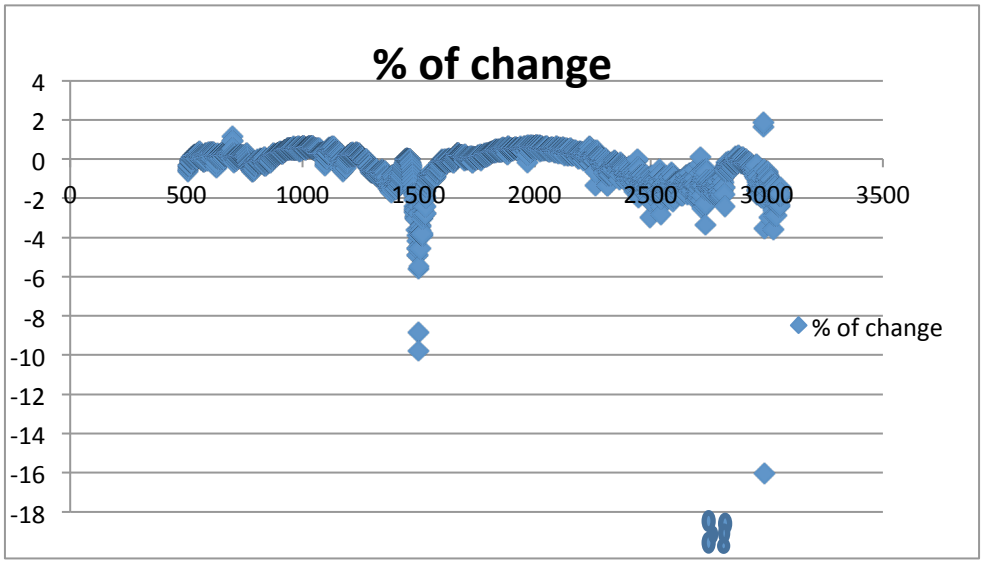

Figure 16 Percentage of change with respect to spectrum using mDF

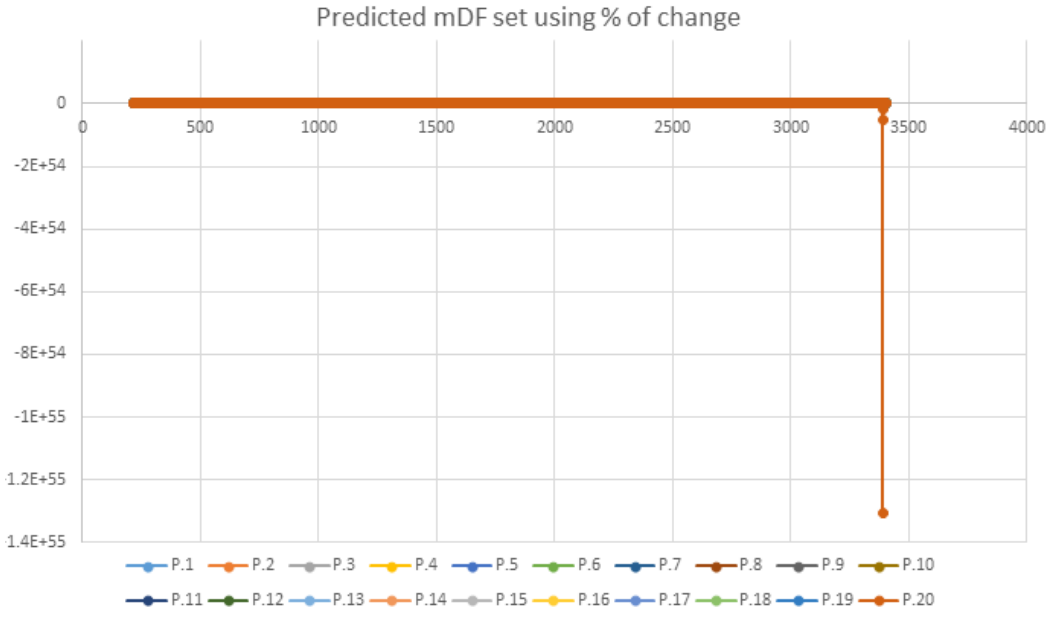

Figure 17 Predicted sample using percentage of difference

2.4 Conclusion

Compared to dewaxed samples, frozen fixed samples (except the control group or frozen fixed sample without fixation) have all featured peaks : They all have peaks caused by C-C-N symmetric stretching from lipids or vibrations of C-O-C rings from carbohydrates at 877cm^{-1}, signal from protein Phe around 1033 cm^{-1}, vibration of (C-O, C, N) at 1128 cm^{-1}, changes of Amide III peak at 1220-1284 cm^{-1} and signal from several kinds of proteins at 1480 cm^{-1}. Moreover, there are signals caused by subtle changes in the secondary structure of protein, change from amide I in protein at 1680-1655 cm^{-1} and signal of CH_2 at 2850 cm^{-1}. Two paraffin fixed sample groups have similar key peaks but frozen fixed samples have spectra with a higher intensity or magnitude. However, it cannot be ruled out that some of the variances observed among samples (paraffin fixed, dewaxed and frozen fixed) might arise from the differences of mice from which the retinal samples were collected.

Comparing samples with paraffin and with paraffin washed off, table 4 gives a clear picture of the improvement on classification accuracy. The average improvement is 15%, which is very promising. Especially with paraffin washed off, the subtle change caused by amide I in protein can be distinguished at 1680-1655 cm^{-1}.

Table 4 Summary of accuracies

Chemical Fixatives	Accuracy from Classification		Improvement
	w/paraffin	W/ paraffin washed off	
Formalin vs Etoh	80%	95%	15%
Formalin vs mDF	75%	90%	15%
Etoh vs. mDF	85%	100%	15%

In conclusion, different fixation protocols do change the spectroscopic features of the samples, evidenced by their differentiation. By washing off paraffin, more key peaks can be recognized, and classified with higher accuracy, which can serve as a reference to explore meaningful biological information. Washed samples have all key peaks as seen in the frozen fixed samples, but the effect caused by chemical fixative cannot be easily rectified by simple mathematical processing. Additionally, these changes have their own chemical implications, which need to be further evaluated in the context of disease vs. healthy comparison.

CHAPTER 3

EVALUATE EFFECTS OF TISSUE FIXATION ON THE DIFFERENTIATION OF DISEASED VS. NORMAL TISSUES

3.1 Introduction

From chapter 2, it has been shown that a simple mathematical correction, to eliminate the effects of fixation, cannot be easily implemented. This is due to the inconsistent variation among different fixation groups and differences among samples. If these parameters are not dealt with caution, they can easily cause over-fitting in discriminant models. Moreover, chemical changes occuring during fixation alter the Raman spectra at a fundamental level. Thus, chemical fixations occuring on the Raman spectra must be assessed alongside observations of the respected diseases.

Over 1 million people in North America suffer from Parkinson's disease, thus, making it the second most common neurodegenerative disease.(Balk, Chung et al. 2006) Parkinson's disease (PD) is chronic and progressive, and the living quality of diseased people is significantly affected from physical, psychological, emotional, social and financial perspectives.(Sharp and Hewitt 2014) Pathologically, Parkinson's diesease may cause the polypeptide chain of α-synuclein to misfold into fiber-like strands, where β-sheets predominate, instead of a unique 3-D structure that confers normal biological funcitons.(Carey 2006) Addtionally, it is observed in the brain of Parkinson's patients the loss of neurons in the substantia nigra in association with proteinaeous deposites that are called lewy body. (Balk, Chung et al. 2006).

Current diagnosis of PD mainly relies on clinial criteria, such as United Kingdom Parkinson's Desease Society Brain Bank Clinical Crtiteria and the National Institute of Neurological Disorder and Stroke. The cardinal motor signs are tremors, rigidity, bradykinesia

and postural instability. These criterias have limitations in detecting PD at early stage as well as in differentiating heterogeneous clinical progression(Kim, Paik et al. 2014). Moreover, other movement disorders have overlaped syptoms aslo decreased the accuracy of diagnosis(Kim, Paik et al. 2014).

Raman spectrosocpy has potential to become an early diagnostic tool for parkinson's diesease; It has been used to characterize structural change of protein, and the chemistry of protein-based deposite in the brain of dead patients(Carey 2006). Raman spectrosocpy can also be used in vitro to trace the changes at early stages on the protein misfolding pathway (Carey 2006, Uversky, Kabanov et al. 2006).

Since the retina is a derivative of forbrain, and it is a part of the nervous system, it is possible to detect chemical changes in the brain through characterizing molecular changes occuring at the retina utilizing molecular imaging techniques. Raman spectroscopy has been explored as a tool for the study of brain disease and retinal disease, such as the study of neuroinflammation (Pablo Villoslada1 2012), Glaucoma (Wang 2011) and age-related macular degeneration.(Howells, Eperjesi et al. 2011). However, most exploratory in vitro studies focused on fixed retinal tissue samples. In most cases, the effects of the fixation processes on the Raman spectra of the samples were not characterized.

Described in chapter 2, chemical fixations may cause fundamental strucutral changes in the Raman spectra, and the effect of which can not be easily eliminated using mathematical modificaiton. Thus, the goal of this chapter is to investigate, under the effect of chemical fixatives, if Raman spectra can be utilized to differentiate diseased samples from normal control samples.

In this effort, with the application of partial least square discriminant analysis (PLS-DS) and Variable Importance Projection (VIP) scores, wavenumbers with spectral differences considered significant between diseased and normal samples are selected or highlighted. These wavenumbers are compared to regions under the influence of chemical fixatives. As a result, the overlapped region(s) can be identified and even eliminated. Subsequently, spectral regions without the impact of chemical fixative are identified and explored for disease diagnosis. A discriminant model was developed based on this approach, and it was successfully applied to differentiate retinal samples from mouses with Parkinson's disease from normal controls with highly improved accuracy.

3.2 Materials and Methods

Three 5-month old mice (ALM 55.2, ALM 62.7, ALM 54.1) were used in this research: ALM 55.2 is genotype control (a particular gene or set of genes carried by a mouse that are directly related to Parkinson's diesease were controlled to be consistant among samples) ; ALM 62.7 is age control (all samples are the same age, from which the influence of different genotype can be studied); and ALM 54.1 is diseased. All retinal samples were fixed by Bouin's fixative and embedded in paraffin. 25 measurements on each mouse retinal sample were taken with the utilizaiton of 780 nm laser. Bouin's fixative is consisted of picric acid, acetic acid and formaldehyde. Bouin's fixative is similar to modified Davidson's fixative (mDF), except that alcohol is replaced by picric acid. Moreover, considering received samples are under either genotype of age controls, it is hard to find new healthy samples that meet all control requirements. For the sake of these reasons, randomly selected samples fixed by mDF are used as a reference to study the effect caused by chemical fixatives.

Data preprocessing includes smoothing, modified polynomial baseline correciton and peak normalizaiton. Followed by the utilizaiton of partial least square discriminant analysis (PLS-DS) and Variable Importance Projection (VIP) scores, regions where significant changes caused by disease can be highlighted by VIP scores and then compared to wavenumbers where alteration caused by chemical fixatives occur.

The general approach can be summarized as four steps:

1. Calculate VIP scores of diseased vs. control groups. This claculation will reveal spectral range which contain the most relevant information that can distinguish diseased from control samples.
2. Calculate VIP scores of mDF vs. frozen fixed groups. This calculation will reavel spectral range which contains the most relevant infpormation that can distinguish chemically-fixed vs. frozen fixed samples.
3. Identify overlapping spectral regions between 1 and 2. Inside these regions, it could be considered that fixation and disease can both have significant effects on the retinal samples, and it would difficult to tell one from the other. From a disease diagnosis standpoint, these regions should be avoided, because the spectral differences observed might not arise from disease, instead it might arise from fixation.
4. After the overlapping regions from 3 are removed, contruct discriminant models to differentiate diseased vs. control groups based on the non-overlapping regions of the spectra which also show significant VIP scores. These are the regions that are heavily influenced by disease, but not so much by fixation. Hence, these are the spectral regions from which a better classification/differentiation can be expected.

The utilization of VIP scores highlights the importance of each wavenumber by their controbution to the final diagnosis. The VIP score summarizes of the importance of the projection when finding the latent variables, and the it is calculated as:

Equaiton 3.1 $$VIP_f = \sqrt{\frac{\sum_{f=1}^{F} w_{jf}^2 SSY_{fJ}}{SSY_{total}F}}$$ (Martin A.B. Hedehaard 2014)

Intensity(j) and wavennumbers(f) can be imagined as a j*f matrix: j is the individual intensity of wavenumber f, and w_{jf} is the weight value for jth intensity at wavenumber f. SSY_f is the sum of squars of explained variances for the *f*th wavenumber, while SSY_{total} is the total sum of squares explained of all intensities. (Martin A.B. Hedehaard 2014) By using PLS-DA, the produced weight (w) can reflect the covariance between wavenumbers and intensities from all samples. Then with the weight being applied to the calculation of VIP scores, the alteration of intensities can be better explaiend and the impact of chemical fixation at eacj wavenmbers can be modeled accurately(Martin A.B. Hedehaard 2014). To read VIP scores, it is important to know the magnitude of each score is proportionally to the level of impact from chemical fixaiton.

3.3 Results

The average spectra of age control group, diseased group, genotype control group and mDF fixed healthy samples are shown in figure 18. All spectra are ploted in a 3-D space, allowing a clear view of difference among all groups. Clearly, the mDF groups shows signigicant difference of peak intensity at 1500 cm^{-1} and 2850 cm^{-1}, which are marked by blue color. However,this difference is hard to differetiate from visual inspection, thus the applicaiton of PLS-DA VIP score is especially meaningful. VIP scores can correlate the disease diagnosis to the intensity at each wavenumber, from which wavenumbers that contribute to either disease or chemical fixaion can be distinguished.

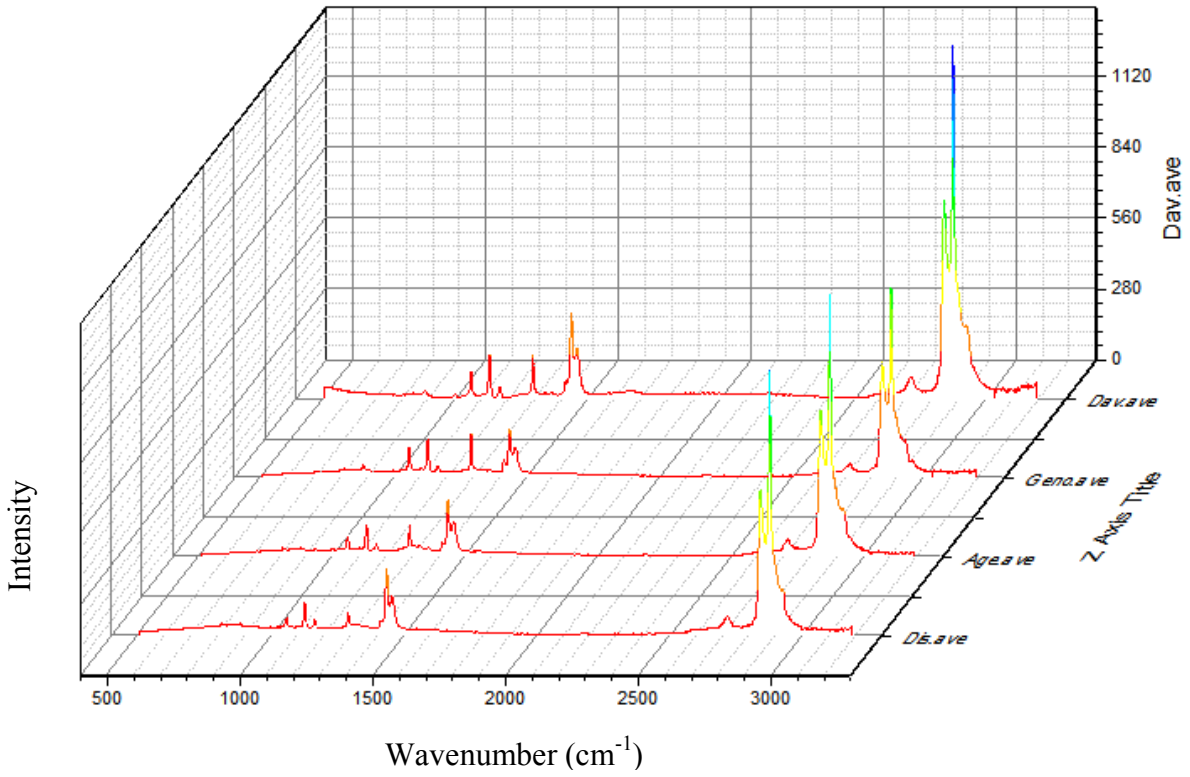

Figure 18 the mean spectra of mDF and Bouin's fixative fixed samples

Plots of VIP scores of the comparison of different control group to diseased group and comparison of frozen fixed and mDF fixed samples can be seen in figure 18. A black line is used to label when vip score equals to 1, and the color gradient from red to blue is used, which corresponds to VIP scores from low to high. In other words, the bluer the color is, the higher the VIP values are. To summarize the change of color gradient, two general regions are marked in black where wavenumbers within this part are important to the classification of disease, when a blue color is used to mark the region where significant alternation is caused by mDF and disease. The overlapped region is between 750 cm^{-1} to 1000 cm^{-1}, by eliminating

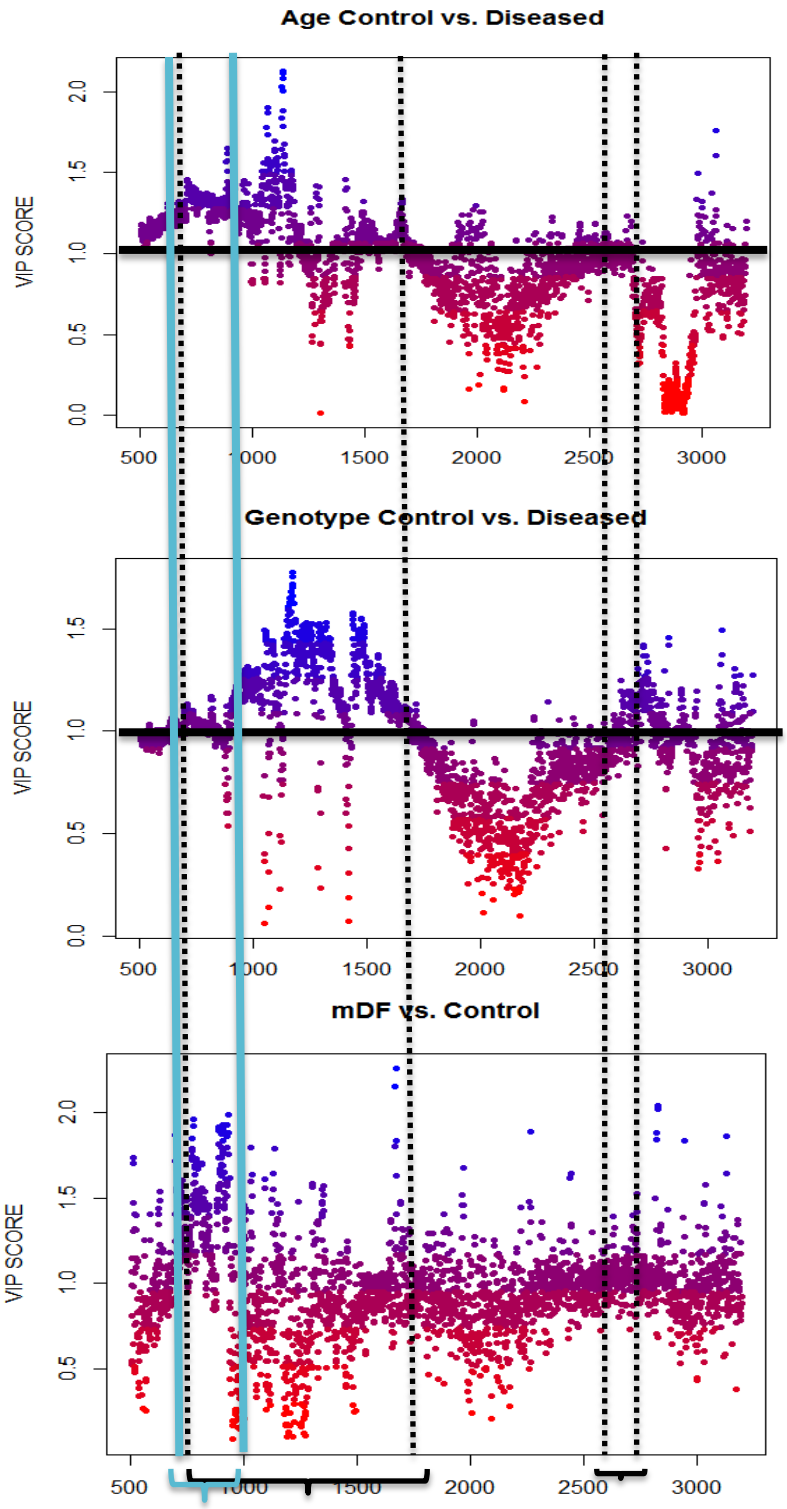

Figure 19 Plots using VIP scores: The region labeled in blue indicates the overlapped wavenumbers where intensity suffers both from the effects of fixation and alternations caused by disease.

which,the diagnosis can become more accurate, as it has less effect from fixation.

The peaks within 750-1000cm^{-1} might not have strong signals, which is hard to be captured as high Raman Intensity but can be observed from high VIP scores. Based on the

Table 5 Peak Assignments

Peak (cm^{-1})	**Assignment**			
	Nucleic Acids	Proteins	Lipids	Carbohydrates
1736			C=O ester	
1680-1655		Amide I	C=C str.	
1617		C=C Tyr, Trp		
1607		C=C Phe, Tyr		
1578	G, A			
1480-1420	G, A, CH def	C-H	CH def	CH def
1342	A, G	C-H		CH def
1320	G	C-H		
1301			CH_2 twist	
1284-1220	T, A	Amide III	=CH bend	
1209		C-C_6H_5. Phe, Trp		
1176		C-H bend Tyr		
1158		C-C/C-N str.		
1128		C-N str.		C-O str
1095-1060	PO_2^- str.		Chain C-C str.	C-O, C-C str
1033		C-H in-plane Phe		
1005		Sym. Ring br Phe		
980		C-C BK str. β-sheet	=CH bend	
937		C-C BK str. α-helix		C-O-C glycos.
877			C-C-N^+ sym str	C-O-C ring
854		Ring br Tyr		
828	O-P-O asym.str.	Ring br. Tyr		
811	O-P-O str. RNA			
788	O-P-O str. DNA			
782	U,C,T ring br			
760		Ring breath Trp		
729	A			
717			$CN^+(CH_3)_3$ str	
667	T, G			
645		C-C twist Tyr		
621		C-C twist Phe		

peak assignment table (table 5), it is possible that chemical fixative alters the strucure of protein by changing the β sheet at 980 cm^{-1}, σ helix at 937cm^{-1} , breaking the ring structure

of tyrosine at 854 cm^{-1} or 828 cm^{-1} and triggers C-C-N symetric streching from lipids or vibrations of C-O-C rings from carbohydrates at 877cm^{-1}.

In figure 19, two comparisons of control vs. Formalin and control vs Etoh using their VIP scores are reported. Clearly, they both have more impacted regions from chemical fixations in blue color as well overlaps with the diagnosing region as calculcated using figure 18, compared to that of the mDF. Thus this results correpond to the idea that mDF is the most appropriate fixative for ocular fixation.

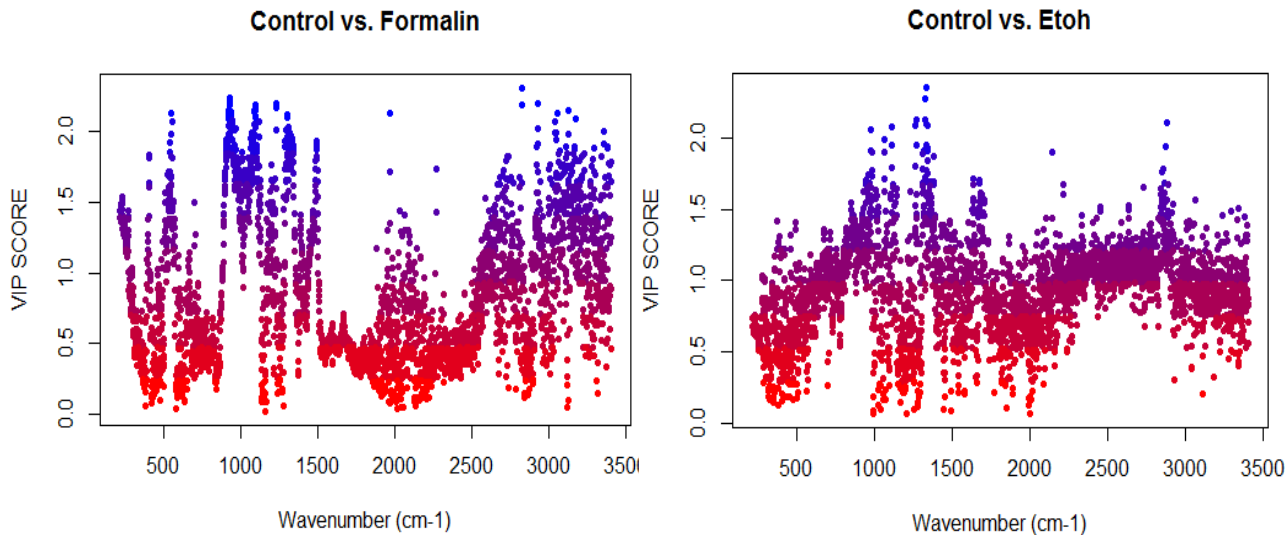

Figure 19. Plots using VIP scores

3.4 Classification Using the Selected Region

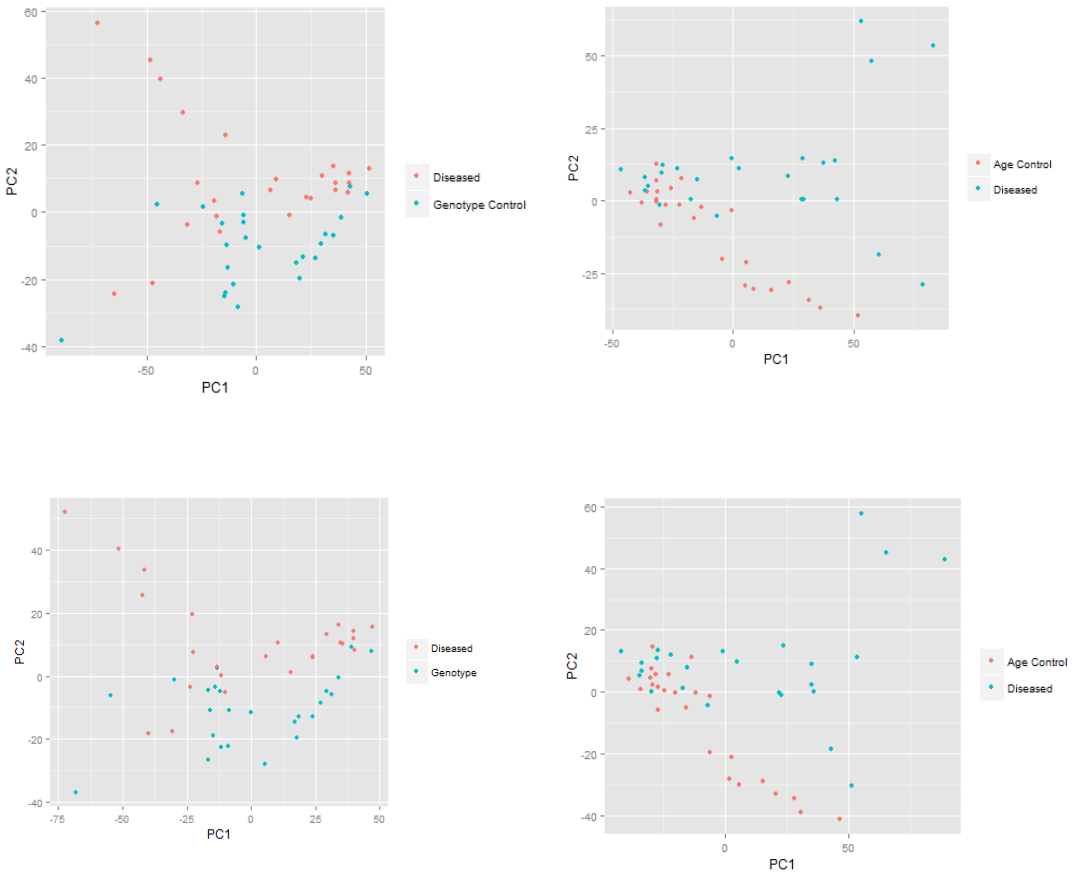

Figure 20. PCA analysis of data w/ and w/o chemical affected regions

The overlapped region of 750-1000 cm^{-1} is eliminated from the spectra data, and figure 19 and table 6 are the summary of the processed data. After running a PCA analysis, figure 20 indicate on a 2-D plane, the removal of the overlapped region does not change the distribution of spectra data. However, the summarized accuracies in table 6 indicate an exceptional improvement on classification.

Table 6 Summarized accuracies of classification using original data and selected data

	Original	Selected	Trend
Accuracy of genotype control vs. diseased	69.23%	100%	Increase
Accuracy of age control vs. diseased	69.23%	92.31%	Increase

3.5 Conclusion

In conclusion, the unitlizaiton of PLS-DA and VIP scores can elminate most of the effect caused by chemical fixative, as well they highlight the regions where alternation caused by disease occur. With further comparion of control vs. Etoh, 10% NBF and mDF respectively, it shows mDF, among three approaches, has the least impact on Raman spectra and proves that mDF is advantageous over conventional fixatives in terms of ocular fixation. This information can be pontetially applied for future disease diagnosis, reulting in a higher and more accurate disease diagnosis result.

Even though Bouin's fixative is not performed on same control samples, this methodology can still serve as a reference for future work: both to investigate the impact under Bouin's fixative and to evalute the quality of specific fixaion in different biological environment, which is not limited to retina. Further improvement can be build upon a larger database, in which more fixation methods can be summarized using samples with controlled and consistent quality. This is exceptionally meaningful since various fixative methods are currently being applied on biological samples without enough inforamion from fixations.

CHAPTER 4

GENERAL CONCLUSION AND FUTURE PERSPECTIVES

In this research, three fixation groups, including frozen control vs. frozen fixed, paraffin embedded control vs. paraffin embedded fixed and dewaxed control vs. dewaxed fixed, were compared based on their Raman spectroscopic characteristics. The result in chapter 2 has shown that simple mathematical correction to eliminate the effects of fixation cannot be easily implemented , since the variation among different fixation groups is not consistent, and differences among samples, if not dealt with caution, can easily cause over-fitting in discriminant models. Moreover, chemical changes are occuring during fixation that alter the Raman spectra at a fundamental level. This brings the need to look at the effect of chemical fixations on Raman spectra in comparison with that brought on by diseases (e.g., Parkinson's disease) in Chapter 3. The unitlizaiton of PLS-DA and VIP scores can elminate most of the effects caused by chemical fixatives, Also these techniques highlight the regions where alternation caused by the disease is the most significant. By using these selected regions in the classification modeling, a higher and more accurate discriminant results that reveal the differences between the diseased and normal control samples with over 20% increasing in accuracies, which potentially can lead to better diagnosis for the disease.

However, the results reported in this thesis are not without weakness. In Chapter 3, since reference samples under the same age control or genotype control were not available, mDF fixed samples were utilized as a control group. Ideally, the same fixation protocol (i.e, Bouin's) should be used to be consistent with the disease vs. normal study. Additionally, other biological environments can also be evaluated, and further development can be

conduced by building a larger database, in which more fixation methods can be investigated using samples with controlled and consistent quality, and the spectral range in which each of the fixation protocol has major influence can be identified and recorded. This will be exceptionally meaningful since various fixative methods are currently being applied on biological samples without enough inforamion on what spectroscopic changes are being caused by the fixation. With this work being done, samples collected and fixed over a long duration can be studied and characterized, so that the feasibility of using Raman spectroscopy to characterize biological and pathological samples can be firmly established to add a new tool to the disposal of pathologists.

REFERENCES

(2000). Handbook of applied multivariate statistics and mathematical modeling / edited by Howard E. A. Tinsley and Steven D. Brown. San Diego, San Diego : Academic.

A.Samuelson, D. (2007). "Textbook of Veterinary Histology." 487.
Abateneh, A., M. Tesfaye, S. Bekele and Y. Gelaw (2013). "Vision Loss and Psychological Distress among Ethiopians Adults: A Comparative Cross-Sectional Study." PLoS One **8**(10): e78335.

Alcamo, I. E. (2009). "Anatomy Coloring Workbook." 142.

Alexandros Kyriakides1, Evdokia Kastanos2, Katerina Hadjigeorgiou1, Costas Pitris1 (2010). "Classification of Raman spectra using the correlation kernel." Journal of Raman Spectroscopy.

Amer, M. S. (2009). Raman Spectroscopy for Soft Matter Applications. Hoboken, N.J.
Balk, E., M. Chung, G. Raman, A. Tatsioni, P. Chew, S. Ip, D. DeVine and J. Lau (2006). "B vitamins and berries and age-related neurodegenerative disorders." Evid Rep Technol Assess (Full Rep)(134): 1-161.

Beattie, J. R., S. Finnegan, R. W. Hamilton, M. Ali, C. F. Inglehearn, A. W. Stitt, J. J. McGarvey, P. M. Hocking and W. J. Curry (2012). "Profiling retinal biochemistry in the MPDZ mutant retinal dysplasia and degeneration chick: a model of human RP and LCA." Invest Ophthalmol Vis Sci **53**(1): 413-420.

Bot. A.C.C., H., A., De Mul, F. F. M., Vrensen, G.F.J.M. and Greve J. (1989). "Raman microspectroscopy of fixed rabbit and human lenses and lens slices: new potentialities " Exp.Eye Res(49).

Carey, P. R. (2006). "Raman crystallography and other biochemical applications of Raman microscopy." Annu Rev Phys Chem **57**: 527-554.

Collette, Timothy W., and Ted L. Williams. "The role of Raman spectroscopy in the analytical chemistry of potable water." Journal of Environmental Monitoring4.1 (2002): 27-34.

Fan, L. and Y. Liu (2013). "Automate fry counting using computer vision and multi-class least squares support vector machine." Aquaculture **380–383**(0): 91-98.

Fullwood, L. M., D. Griffiths, K. Ashton, T. Dawson, R. W. Lea, C. Davis, F. Bonnier, H. J. Byrne and M. J. Baker (2014). "Effect of substrate choice and tissue type on tissue preparation for spectral histopathology by Raman microspectroscopy." Analyst **139**(2): 446-454.

GEORG SCHULZE, A. J., * MARCIA M. L. YU, ARNEL LIM, ROBIN F. B. TURNER,† and MICHAEL W. BLADES (2005). "Investigation of Selected Baseline Removal Techniques as Candidates for Automated Implementation." **59**: 545-574.

Harris, J. "Rewiring Neuroscience."

Hart, J. D. (1997). Nonparametric smoothing and lack-of-fit tests / Jeffrey D. Hart. New York, New York : Springer.

Hassel, J. a. H., A.R. (1974). "Histochem." Cytochem. **22**: 229-239.
Henderson, T. (1996). "The eye."

Hollyfield, B. A.-A. a. J. G. (2010). "Developmental Anatomy of the Retinal and Choroidal Vasculature." Elsevier.

Howells, O., F. Eperjesi and H. Bartlett (2011). "Measuring macular pigment optical density in vivo: a review of techniques." Graefes Arch Clin Exp Ophthalmol **249**(3): 315-347.

Howroyd, P., R. Hoyle-Thacker, O. Lyght, D. Williams and E. Kleymenova (2005). "Morphology of the fetal rat testis preserved in different fixatives." Toxicol Pathol **33**(2): 300-304.

Huo, H.-B., X.-J. Zhu and G.-Y. Cao (2006). "Nonlinear modeling of a SOFC stack based on a least squares support vector machine." Journal of Power Sources **162**(2): 1220-1225.

Kelder, W., B. Inberg, J. T. M. Plukker, H. Groen, P. C. Baas and A. T. M. G. Tiebosch (2008). "Effect of modified Davidson's fixative on examined number of lymph nodes and TNM-stage in colon carcinoma." European Journal of Surgical Oncology (EJSO) **34**(5): 525-530.

Kim, D., J. H. Paik, D.-W. Shin, H.-S. Kim, C.-S. Park and J.-H. Kang (2014). "What is the Clinical Significance of Cerebrospinal Fluid Biomarkers in Parkinson's disease? Is the Significance Diagnostic or Prognostic?" Exp Neurobiol **23**(4): 352-364.

Kniggendorf, A. K., T. W. Gaul and M. Meinhardt-Wollweber (2011). "Effects of ethanol, formaldehyde, and gentle heat fixation in confocal resonance Raman microscopy of purple nonsulfur bacteria." Microsc Res Tech **74**(2): 177-183.

Kolb, H. (2007). "The Organization of the Retina and Visual System ".

Latendresse, J. R., A. R. Warbrittion, H. Jonassen and D. M. Creasy (2002). "Fixation of testes and eyes using a modified Davidson's fluid: Comparison with Bouin's fluid and conventional Davidson's fluid." Toxicologic Pathology **30**(4): 524-533.

Leger, M. N. R., Alan G. (2006). "Comparison of Derivative Preprocessing and Automated Polynomial Baseline Correction Method for Classification and Quantification of Narcotics in Solid Mixtures." **60**(2): 32A-56A and 109-228

Lukasiewicz, P. D. (2013). "Adler's Physiology of the Eye." Elsevier.

Mahadevan-Jansen, C. A. L. a. A. (2003). "Automated Method for Subtraction of Fluorescence from Biological Spectra." Applied Spectroscopy **57**.

Manly, B. F. J. (1944). "Multivariate statistical methods: a primer."

Martin A.B. Hedehaard, K. L. C., Christine-Maria Horejs and Molly M. Stevens (2014). "Model based vatiable selection as a tool to highlight biological differences in Raman spectra of cells." Analyst(139): 4629.

Matsuda, Y., T. Fujii, T. Suzuki, K. Yamahatsu, K. Kawahara, K. Teduka, Y. Kawamoto, T. Yamamoto, T. Ishiwata and Z. Naito (2011). "Comparison of Fixation Methods for Preservation of Morphology, RNAs, and Proteins From Paraffin-Embedded Human Cancer Cell-Implanted Mouse Models." Journal of Histochemistry and Cytochemistry **59**(1): 68-75.

Morawietz, G., C. Ruehl-Fehlert, B. Kittel, A. Bube, K. Keane, S. Halm, A. Heuser and J. Hellmann (2004). "Revised guides for organ sampling and trimming in rats and mice - Part 3: A joint publication of the RITA*) and NACAD**) groups." Experimental and Toxicologic Pathology **55**(6): 433-449.

Notingher, I. H., L.L. (2006). "Raman microspectroscopy: a noninvasive tool for studies of individual living cells in vitro." Med.Devices(3): 215-234.

Ollivier, F. J. (2004). "Comparative morphology of the tapetum lucidum (among selected species)." Wiley

Pablo Villoslada1, M. M., Alice Taubes3, Beatriz Moreno4 and Dimitri Petrov5 (2012). "Raman Spectroscopy Analysis of the Retina Reveals Changes in Glutamate, N-Acetyl-Aspartate, NADH and Phosphatidylcholine in Neuroinflammation (P01.166)." Neurology(78): 1109.

PAYAM REFAEILZADEH, L. T., HUAN LIU (2008). "Cross-Validation."

Pearse (1968). "In Histochemistry: Theoretical and Applied. ." Churchill Livingstone **1**.

Raman, C. V. K., K. S. (1928). "A new type of secondary radiation." Nature(121): 501-502.
Richards-Kortum, R. and E. Sevick-Muraca (1996). "Quantitative optical spectroscopy for tissue diagnosis." Annu Rev Phys Chem **47**: 555-606.

ROESSL, U. (2014). "In Situ Protein Secondary Structure Determination in Ice: Raman Spectroscopy-Based Process Analytical Tool for Frozen Storage of Biopharmaceuticals." Pharmaceutical Biotechnology.

Shao, Y., Y. Cen, Y. He and F. Liu (2011). "Infrared spectroscopy and chemometrics for the starch and protein prediction in irradiated rice." Food Chemistry **126**(4): 1856-1861.

Sharp, K. and J. Hewitt (2014). "Dance as an intervention for people with Parkinson's disease: A systematic review and meta-analysis." Neurosci Biobehav Rev.

Suykens, J. A. K. (2002). Least Squares Support Vector Machines. River Edge, NJ.
Tinsley, H. E. A. (2000). "Handbook of Applied Multivariate Statistics and Mathematical Modeling."

Uversky, V. N., A. V. Kabanov and Y. L. Lyubchenko (2006). "Nanotools for Megaproblems: Probing Protein Misfolding Diseases Using Nanomedicine Modus Operandi." Journal of proteome research **5**(10): 2505-2522.

Wang, Q. (2011). "Exploring Raman spectrosocopy for the evaluation of glaucomatous retinal changes." Biomedical optics(16): 10.

Warwick, R. (1976). "Eugene Wolff's Anatomy of the Eye and Orbit."

Wei-Chuan Shih, K. L. B., and Michael S. Feld (2007). "Non-invasive Glucose Sensing with Raman Spectroscopy ".

Zhang, S.-L. (2012). Raman Spectroscopy and its Application in Nanostructures. HobokenChichester, West Sussex, Hoboken John Wiley & Sons.

Zhang, Z.-M. (2009). "An intelligent background-correction algorithm for highly fluorescent samples in Raman spectroscopy." Wiley Interscience.